Utrecht University

Submarines Lobe Geometry and the Average Grain Size Distribution Prediction based on Its Channel System

Master Thesis Report

Department of Earth Science

Utrecht University

Vicky Ruliansatri

6117651

Supervisors:

Dr. Joris T. Eggenhuisen

Dr. João Trabucho Alexandre

Abstract:

Submarine lobes are one of the favorable reservoir targets for hydrocarbon exploration and production. However, predicting the lobes geometry in the subsurface remains uncertain due to their complex geometries and limitation of existing subsurface data sets to define the internal architecture and the facies distribution of submarine lobes deposits.

An analytical model, so-called Sediment Budget Estimator-Lobe (SBE-Lobe), is developed to predict the geometry of submarine lobes and the average grain-size distribution along their long axis. Lobes architecture is quantified based on the vertical grain size stratification, the velocity structure and the channel feeding configuration. The model development is started by integrating the Rouse Equation on to the SBE-Channel module, a process-based turbidity current model developed by Eggenhuisen et al. (2019a), to obtain complete series of concentration profile for all grain size classes. Subsequently, lobe geometry is predicted using the advection length approach.

The modeling result is displayed in 2D. Validation of the model against the laboratory experiment suggests that this model can be used as the first-order prediction of lobe geometry. The model can locate the depositional area of the fine sand and very fine sand grain size class. It also provides a relatively good estimation of lobe thickness in the middle and distal areas. This model can be compared against bed and lobe element geometries that comprise of weakly compensational beds.

Application of the SBE-Lobe to the ancient turbidite deposit has shown its consistency in predicting the sediment budget and its ability to predict the submarine lobe geometry and the average grain-size distribution based on the channel system within the amplitude of field data. Therefore, this tool potentially can be applied to the subsurface evaluation for predicting the gross reservoir volume, localize the potential area, and defining the reservoir boundary.

However, the model still has limitations in predicting apex lobe geometry. The model appears to overestimate the lobe thickness in the proximal region and underpredict the sediment transport distance of the coarser particles. Future research should, therefore, aim to improve the model by incorporating the dynamic process that occurs in the channel lobe transition zone (CLTZ) into the model and coupling the effect of the temporal and spatial evolution of the flow velocity.

Keywords: submarine lobes, analytical model, the Rouse Equation, advection length, submarine lobe geometry prediction, subsurface evaluation

Contents

List of Figures

List of Tables

1. Introduction

Submarine lobes, components of submarine fans (**Figure 1a**), form at the end of feeder channels where turbidity currents lose their competence to transport some or all of their load (Deptuck and Sylvester, 2018). They represent the final product of sediment deposition (Prélat et al., 2010). Conventionally, submarine lobes deposits were described as radial bodies which are thinner and finer-grained towards the distal basin (e.g., Mutti, 1977; Bouma, 2000).

From an economic perspective, deep-water lobes play an important role in the petroleum system elements. These sediment bodies are one of the favourable reservoir targets for hydrocarbon exploration and production. Therefore, lobe characteristics such as dimensions, geometries, and grain-size distributions become of interest to study to improve an understanding in the reservoir prediction (Mulder and Alexander, 2001; Portén et al., 2017). However, these systems are challenging to model.

Deepwater lobes have complex geometries as a result of the interaction between internal and external factors (e.g., Fildani and Normark, 2004; Deptuck et al., 2008; Prélat et al., 2009; Spychala et al., 2017a). Moreover, submarine lobes systems are commonly exposed as an outcrop partially, and existing subsurface data sets have a limitation to define the internal architecture and the facies distribution of submarine lobes deposits (Fildani and Nomark, 2004; Prélat et al., 2010). In addition to that, they are poorly imaged in the seismic section as a result of their internal characteristic that mostly has a chaotic pattern, seismic resolution issue and low acoustic impedance contrast. These factors lead to the uncertainty in defining the dimension of the submarine lobes, which is related to risk in subsurface evaluation. Hence, the need for accurate prediction tool of lobe deposits such as their geometry and spatial grain size distribution is required.

This research is performed to construct an analytical model, so-called the Sediment Budget Estimator-Lobe (SBE-Lobe), to predict the geometry of submarine lobes and the average grain-size distribution along their long axis. We quantify lobes architecture based on the vertical grain size stratification, velocity structure, and the channel feeding geometry of the turbidity currents that flow onto the lobe (**Figure 1b, 1c, and 1d**). The basis of model development is the Sediment Budget Estimator-Channel (SBE-Channel), a process-based turbidity current model developed by Eggenhuisen et al. (2019a). However, the SBE-Channel needs to be modified by

replacing the simple decay equation with the Rouse Equation to obtain a complete set of concentration profiles for all grain size classes that required for the development of the SBE-Lobe.

The objectives of the presented research are 1) to integrate the Rouse Equation into the SBE-Channel simulation tool, 2) to develop the submarine lobes prediction model, 3) to assess the prediction model accuracy, 4) to investigate the application of the analytical model on Gold Channel, Tres Pasos Formation, Chile, and Lobe 5 of the Fan 3, Skoorsteenberg Formation, Karoo Basin, South Africa.

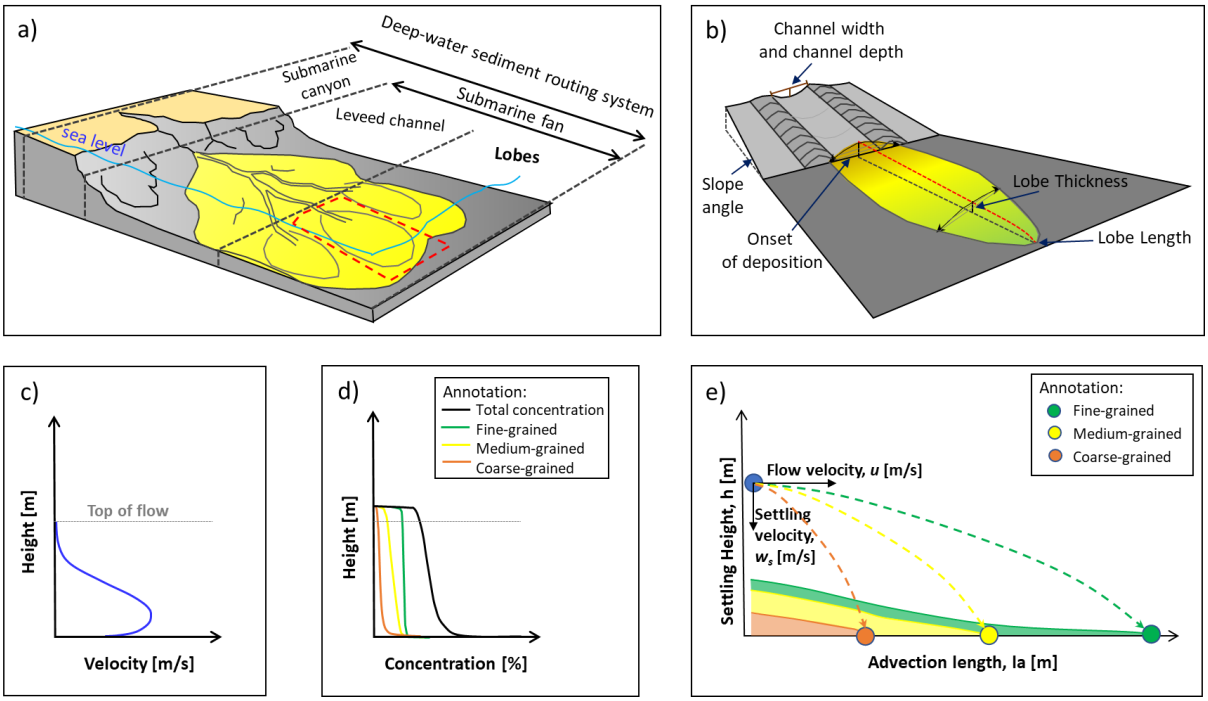

Figure 1. a) Overview of deep-water depositional system, the focus of this research is represented by the red-dash square (modified from de Leeuw et al., 2017), b) Schematic representation of the submarine channel system and fan lobes geometries, which illustrate inputs and outputs of the developed model, c) Typical velocity profile of turbidity current that flow through the submarine channel, d) Sediment concentration profiles for sediments of different grain sizes suspended in the same flow and total concentration profile. These profiles are for the Rouse Equation, e) Illustration of the advection length method that use to predict fan lobes geometry and their spatial grain-size distribution

The submarine lobe geometry is predicted using the advection length approach (**Figure 1e**), which is the simplest process controlling deposition from turbidity currents where settling of sediment that makes up the concentration profile at the channel mouth while the flow travels over the lobe. This simple approximation has been proved through a laboratory flume

experiment that can be used as a first-order estimation tool for down-flow length with an average of approximately 50% accuracy (Spychala et al., 2019).

The model is built with several simplifications. We are ignoring the temporal and spatial evolution of the flow velocity, assuming flat basin floor topography and point-source supplying system (*sensu* Reading and Richards, 1994).

The detailed process in developing the submarine lobe model is described in Chapter 2. Next, Chapter 3 discussed the validation of the modeling result against the flume experiment conducted by de Leeuw et al. (2018) to assess the model accuracy. Afterward, Chapter 4 explained the application of the model to the natural systems. Two systems modeled in this research are Gold Channel, TrePasos Formation, Chile and Lobe 5 of Fan 3, Skoorsteenberg Formation, Karoo Basin, South Africa. Finally, Chapter 5 is summaries and conclusions.

2. Model Development

The SBE-Channel is a process-based turbidity current model to estimate the amount of sediment transported through submarine channel from slope to basin floor fans over a geological timescale. The outputs of this tool are the flow structure, the concentration profile, and the sediment budget estimation. In this research, we used this information to develop a new module to predict the geometry of submarine lobes and the average grain-size distribution along their long axes which called the SBE-Lobe (**Figure 2**). In addition to that, we also extend the previous modification of the sediment concentration profile to obtain a complete set of concentration profiles for all grain size classes and the sediment budget estimation of each grain-size class. This process is done by introducing the Rouse Equation in sediment concentration profile generation.

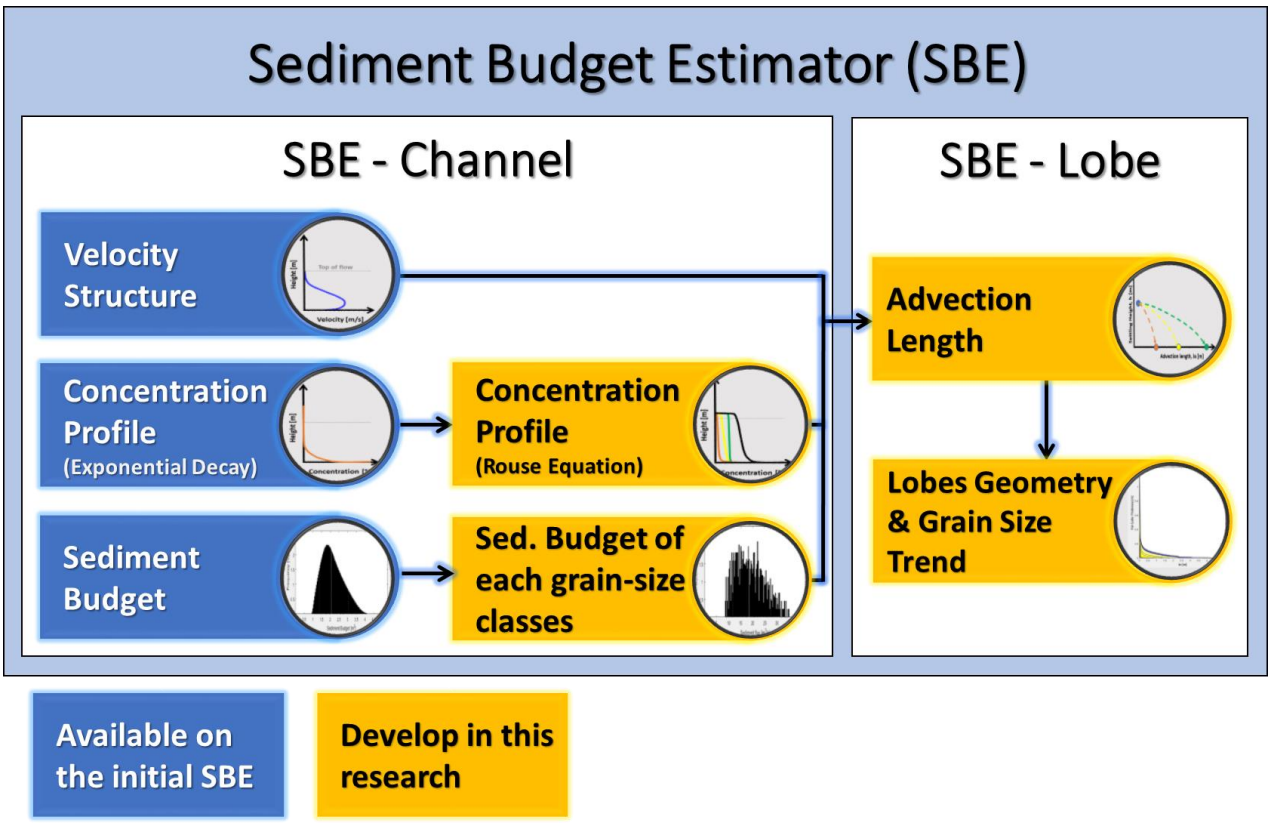

Figure 2. The Sediment Budget Estimator and the output of the SBE-Channel and the SBE-Lobe

2.1. Modification of the SBE-Channel

2.1.1. The Origin of the SBE-Channel

The geological parameters required for the SBE-Channel simulation are grouped into dynamic flow properties and flow duration. Together with pre-define simulation parameters (***Appendix 1***), the dynamic flow properties are used to generate the characteristics of turbidity currents, which consists of velocity structures (**Figure 1c**) and sediment concentration profiles (**Figure 1d**). Multiplication of the velocity structure and the sediment concentration profile produce the sediment flux. Finally, the sediment flux is multiplied by the current duration and current frequency to get the sediment budget estimation over a geological period.

The velocity u [m/s] is a function of logarithmic velocity profile to the flow depth H (u_{log}), and superposing the mixing layer structure throughout the flow from the bed to the top u_{PML} (Eq. 1). This is the standard analytical solution for turbidity current velocity profile and the SBE-Channel calculated it from given channel geometry (see Eggenhuisen et al., 2019a for details).

$$u(z) = u_{log}(z) - u_{PML}(z) \quad \text{(Eq. 1)}$$

The sediment concentration profile c at elevation z [-], is built from an exponential decay function:

$$c(z) = C_b e^{-kz} \quad \text{(Eq. 2)}$$

where C_b is the sediment concentration at the base of the flow [-], and k is decay constant [1/m].

2.1.2. The Grain Size Stratification

The exponential decay function used in the initial SBE-Channel to generate the sediment concentration profile is independent of the grain-size units. This function also does not consider the distribution of different grain sizes in the water column. To include the grain size information, Novianti (2019) has integrated the Rouse Equation into the SBE-Channel. However, Novianti's model only limited to three-grain size values (D_{10}, D_{50}, and D_{90}) which is mean her approach is not enough to model all the available grain-size classes in the flow. Therefore, further improvement is presented in this study by applying the Rouse Equation to all available grain-size classes.

The general workflow for generating the sediment concentration profile is adopted from Novianti (2019) where the profiles are generated through five stages (**Figure 3**). Some modifications are mare to this process by presenting the available sediment in pre-defined classes and generating the profile for all grain-size. So that, complete sets of sediment concentration profiles for all grain size classes can be modeled with the Rouse Equation.

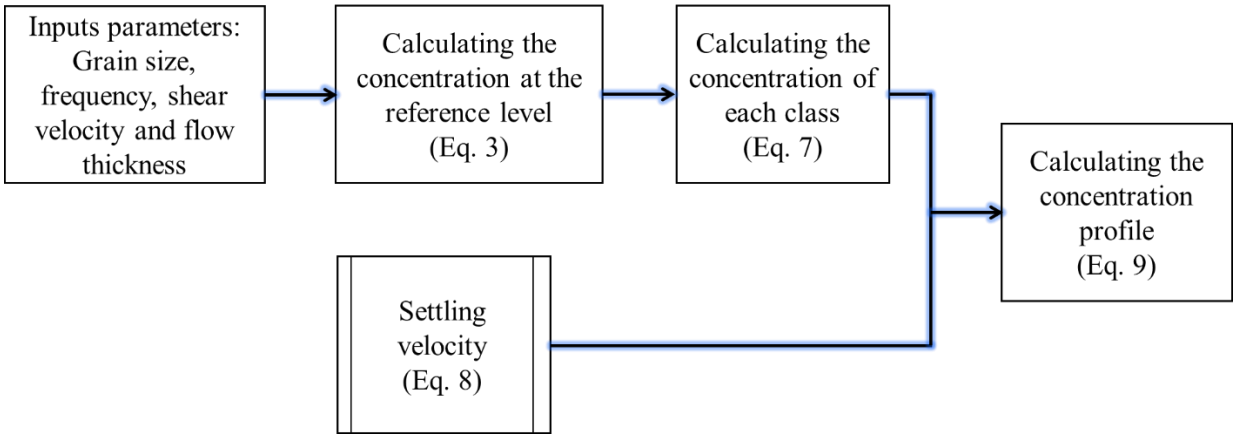

Figure 3. The general process for generating the sediment concentration profile. This workflow is adopted from Novianti (2019) with certain modifications.

The Rouse Equation is widely used to model the concentration profile of turbidity current (Hiscott et al., 1997; Straub and Mohrig, 2008; Bolla Pittaluga and Imran, 2014; Jobe et al., 2017). This classic formulation is still found to be a satisfactory approximation of suspended sediment concentration (Garcia, 2008; Bolla Pittaluga and Imran, 2014). Eggenhuisen et al. (2019b) also further evaluate this equation by setting up the flume experiment and indicates that with certain notice it can be applied for turbidity current.

1. **Define the input parameters**

   The input parameters are consisting of the grain-size and its fraction, shear velocity, and the flow thickness. Grain-size and its fraction are determined from the respective sample of turbidity channel deposits by means of the grain-size distribution analysis. A sample is suggested to be taken from the base of submarine channel deposits since this point is the most representative part where particles are primarily concentrated during the process of sediment deposition. Detail explanation about the procedure of grain-size analysis is described in Novianti (2019).

Table 1. The illustration of the grain-size classes used in the simulation. The frequency and the percentage are for the sample AX30

No	Grain size term	Phi Term		Grain size (mm)		Frequency	Percentage
1	Clay	9	8.75	0.0000	0.0023	0	0
2		8.75	8.5	0.0023	0.0028	0	0
3		8.5	8.25	0.0028	0.0033	0	0
4		8.25	8	0.0033	0.0039	0	0
5	vf silt	8	7.75	0.0039	0.005	0	0
6		7.75	7.5	0.005	0.006	0	0
7		7.5	7.25	0.006	0.007	0	0
8		7.25	7	0.007	0.008	0	0
9	f silt	7	6.75	0.008	0.009	0	0
10		6.75	6.5	0.009	0.011	0	0
11		6.5	6.25	0.011	0.013	0	0
12		6.25	6	0.013	0.016	0	0
13	m silt	6	5.75	0.016	0.019	0	0
14		5.75	5.5	0.019	0.022	0	0
15		5.5	5.25	0.022	0.026	2	0.73
16		5.25	5	0.026	0.031	0	0
17	c silt	5	4.75	0.031	0.037	1	0.37
18		4.75	4.5	0.037	0.044	2	0.73
19		4.5	4.25	0.044	0.053	3	1.10
20		4.25	4	0.053	0.063	8	2.93
21	vf sand	4	3.75	0.063	0.074	7	2.56
22		3.75	3.5	0.074	0.088	12	4.40
23		3.5	3.25	0.088	0.105	15	5.49
24		3.25	3	0.105	0.125	21	7.69
25	f sand	3	2.75	0.125	0.149	29	10.62
26		2.75	2.5	0.149	0.177	26	9.52
27		2.5	2.25	0.177	0.210	38	13.92
28		2.25	2	0.210	0.250	24	8.79
29	m sand	2	1.75	0.250	0.297	34	12.45
30		1.75	1.5	0.297	0.354	25	9.16
31		1.5	1.25	0.354	0.420	12	4.40
32		1.25	1	0.420	0.500	8	2.93
33	c sand	1	0.75	0.500	0.595	3	1.10
34		0.75	0.5	0.595	0.707	1	0.37
35		0.5	0.25	0.707	0.841	1	0.37
36		0.25	0	0.841	1.000	0	0
37	vc sand	0	-0.25	1.000	1.189	0	0
38		-0.25	-0.5	1.189	1.414	0	0
39		-0.5	-0.75	1.414	1.682	0	0
40		-0.75	-1	1.682	2.000	0	0
41	vf pebble	-1	-1.25	2.000	2.378	0	0
42		-1.25	-1.5	2.378	2.828	0	0
43		-1.5	-1.75	2.828	3.364	0	0
44		-1.75	-2	3.364	4.000	0	0
45	f pebble	-2	-2.25	4.000	4.757	0	0
46		-2.25	-2.5	4.757	5.657	0	0
47		-2.5	-2.75	5.657	6.727	0	0
48		-2.75	-3	6.727	8.000	0	0
49	m pebble	-3	-3.25	8.000	9.514	0	0
50		-3.25	-3.5	9.514	11.314	0	0
51		-3.5	-3.75	11.314	13.454	0	0
52		-3.75	-4	13.454	16.000	1	0.37

The grain-size is set up into 52 groups ranging from clay to medium pebble which already covered a typical particle size in turbidity current (**Table 1**). The purpose of pre-defined grain-size ranges is to maintain a consistent number of grain-size bins during the simulation and also allow us to compare the simulations of different systems and channels directly. Representing the grain-size in a spectrum rather than the single grain-size value (such as D_{10}, D_{50}, and D_{90}) also reduces bias in displaying the relative portion of the individual particle.

The grain size distribution data used in the model development are taken from the analysis of the turbidity-current deposit of the Gold Channel, Magallanes Basin, Southern Chile. The samples are collected by de Leeuw (2018), which further being analyzed by Novianti (2019). For illustration purposes, **Figure 4** shows an example of the grain size distribution of the AX-30 sample. This sample is used in Chapter 2 to reconstruct ancient turbidity currents and predict their lobe characteristics.

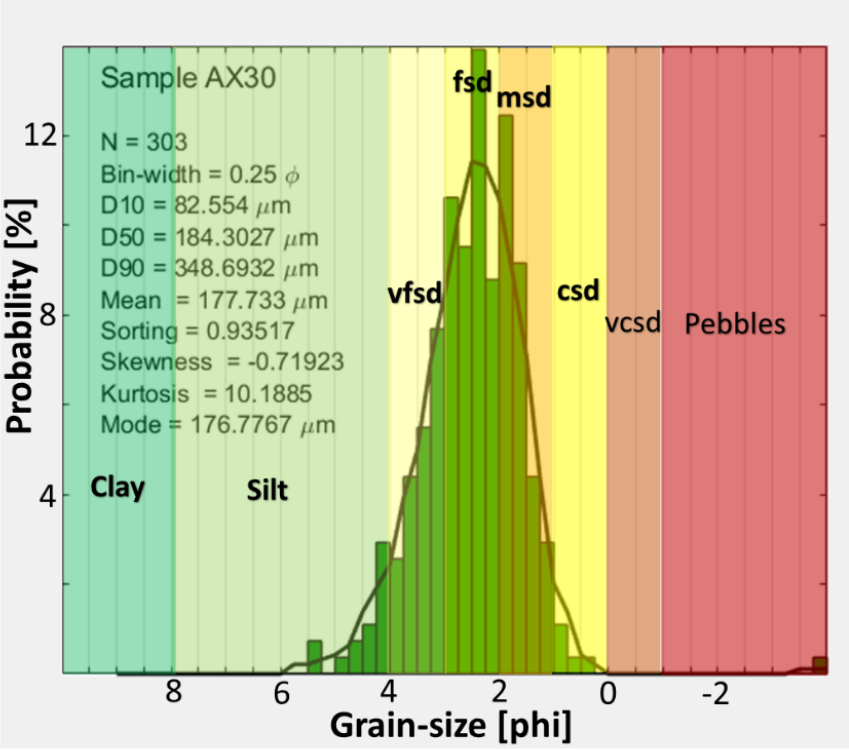

Figure 4. Illustration of the grain size distribution data ranging from clay to medium pebble. The grain size is grouped into 52 classed with 0.25 bin width.

For the calculation of the sediment concentration profile, the elevation limit of the Rouse Equation is set to 1.3 times the flow thickness as defined in the velocity profile. This setting is based on the quantification analysis of turbidity current thickness relative to the channel's depth performed by Mohrig & Buttles (2007). While the shear velocity is already calculated in the SBE-Channel.

From the grain-size distribution analysis, we can calculate the fraction of each grain-size classes i (F_{refi}) with respect to the total grain size. The relative frequencies observed in the sample of channel deposits are assumed to represent the relative frequencies of sediment suspended at the base of the flow.

2. Calculating the sediment profile at a reference level

The sediment concentration at the base of a bypassing turbidity current is calculated using the equation derived by Eggenhuisen et al. (2017) as follows.

$$C_{ref} = \frac{u_*^3}{140\, v\, g\, R} \quad \text{(Eq. 3)}$$

$$u_* = \sqrt{H_r \bar{C} g R S} \quad \text{(Eq. 4)}$$

$$v = \frac{vuw}{rhow} \quad \text{(Eq. 5)}$$

$$R = \frac{(rhos - rhow)}{rhow} \quad \text{(Eq. 6)}$$

Where u_* is the shear velocity [m/s]; v is the kinematic viscosity of water at 20^0 C [m^2/s]; g is gravity acceleration [m/s^2]; R is the relative specific density of sediment in the water [-]; H_r is the hydraulic radius [m]; $\bar{C}$ is the depth-averaged sediment concentration; S is tangent of the slope angle [-]; vuw is the dynamic viscosity of water at 10^0 C [Kg/ms]; $rhos$ is grain density [kg/m^3]; $rhow$ is water density [kg/m^3]. v, g and R value applied in the calculation is 1 x 10^{-6} m^2/s, 9.81 m/s^2, and 1.65 respectively. More simulation parameters used in the simulation are shown in ***Appendix 1.***

Next, the sediment concentration of grain-size class i at the reference level (c_{refi}) is derived from the multiplication of the fraction of each particle size at the reference level with the sediment concentration at the base of the flow (c_{ref}).

$$c_{refi} = F_{refi}(z)\ x\ c_{ref} \quad \text{(Eq. 7)}$$

3. Calculating the settling velocity

The settling velocity v_{si} is the velocity with which specific particles settle in the water. In this study, it is calculated using the equation derived by Ferguson & Church (2004).

$$v_{si} = \frac{R\ g\ D^2}{C1\ v + (0.75\ C2\ R\ g\ D^3)^{0.5}} \quad \text{(Eq. 8)}$$

Where $C1$ is the constant in Stokes' equation of laminar settling [-]; $C2$ is the constant drag coefficient of particle Reynolds number exceeding 10^3 [-]. The value is depending on the roundness of the particle. The suggested coefficient for natural sands is 18 and 1, respectively (Fergusson & Church, 2004) and D is grain-size particle [m].

4. Calculating the concentration profile

The final step is generating the sediment concentration profile of each grain-size class using the Rouse Equation.

$$C_i(z) = C_{refi}\left(\frac{H-z}{z}\left(\frac{z_{ref}}{H-z_{ref}}\right)\right)^{\frac{v_{si}}{\beta k u^*}} \quad \text{(Eq. 9)}$$

Where C_{refi} is the volumetric concentration of suspended sediment [-] in grain class i at the reference level z_{ref} [m], H is the flow thickness [m], z is the elevation above the bed [m], k is the von Karman constant (0.4), $\frac{v_{si}}{\beta k u^*}$ also known as the Rouse number z. The schematic concentration profile in which C_{ref}, H, z, and z_{ref} are shown in **Figure 5**.

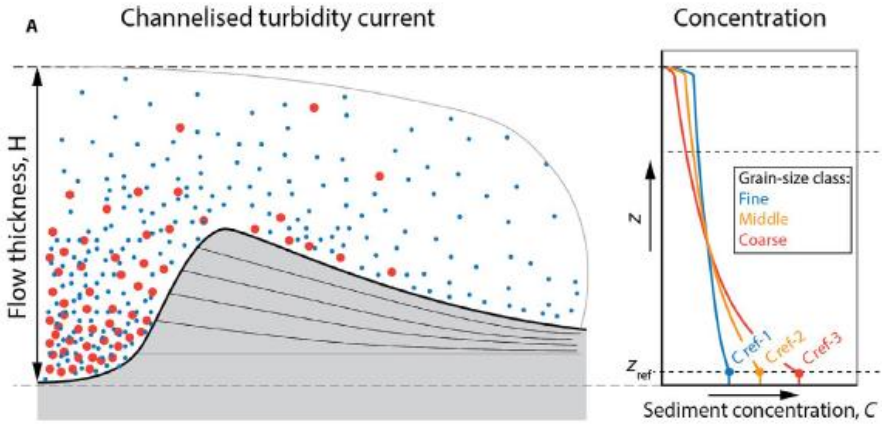

Figure 5. Conceptual model of grain-size stratification in channelized turbidity currents. Left: Schematic representation of a leveed channel. Right: Concentration profiles for different grain-size classes. (adapted from Eggenhuisen et al., 2019b)

2.1.3. New Sediment Concentration Profile and the Comparison

To validate and test the new function, the sediment concentration profile from the Rouse Equation is compared with the profile derived from the exponential decay function (**Figure 6**). The profiles are generated under the same boundary conditions as shown in **Table 2** and ***Appendix 1***. While the exponential decay function only reveals a single concentration profile, the new modified script generates the sediment concentration profile of each grain size as a function of elevation, which also reflects the grain size stratification. For simplification, the profiles derived from the Rouse Equation are shown in eight different grain size terms.

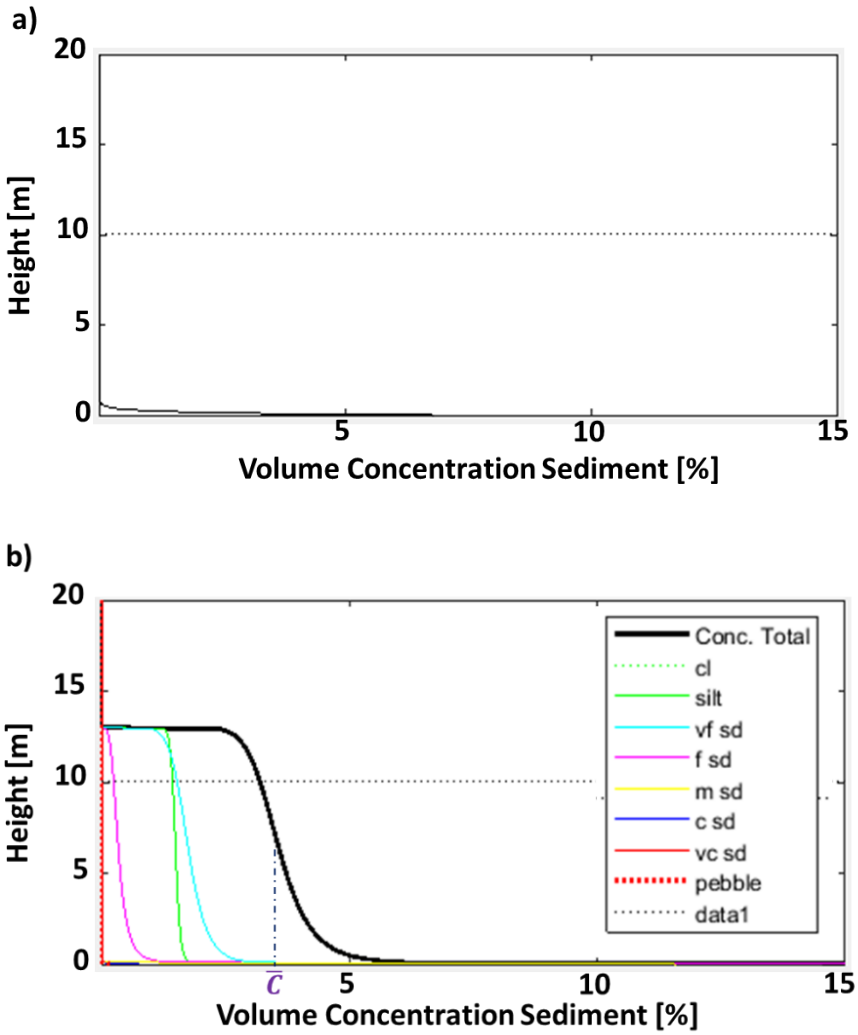

Figure 6. Sediment Concentration Profile: a) Obtained from exponential decay function, b) Obtained from the Rouse Equation before normalization, the average total sediment concentration $\bar{C}$, is 3.5 %. Data 1 in the graph is representing the channel depth

Based on the new sediment concentration profile, most sediments are concentrated at the base of the flow, and the concentration decrease as a function of elevation. The fine-grain material (smaller than very fine sand) is less stratified and disperse fairly homogenous in the flow. On the other hand, the coarser grain size is very well stratified and mostly located at the base of the turbidity current, particularly for particles that coarser than the medium sand. It indicates that the coarser materials are transported near the bed because the current is not strong enough to suspend the coarser particle. It also suggests that in the turbidity current; the suspension is dominated by smaller than very fine sand particles, fine sand grain can be transported as bedload or suspended load mechanism depend on its concentration, while the coarser grain is transported as a bed load. This observation is aligned with the model developed by Eggenhuisen et al. (2019b) (**Figure 5**).

2.1.4. Normalization of New Sediment Concentration Profile

Nevertheless, the profile created by the Rouse Equation produces an average total sediment concentration ($\bar{C}$) that is too high in comparison to the initial set up condition (C_{in}). The average sediment concentration from the Rouse Equation is 3.5 %, which is about ten times higher than the initial input of sediment concentration, 0.3 – 0.6 % (**Table 2**). This overestimation will also lead to the over-predicted of the sediment budget estimation. We solve this issue by applying data normalization.

The normalization is conducted by multiplying the sediment concentration (C_i) with the define constant k_{norm}. This constant is derived from the average total sediment concentration ($\bar{C}$) over the average of initial concentration ($\overline{C_{in}}$).

$$k_{norm} = \frac{\bar{C}}{\overline{C_{in}}} \quad \text{(Eq. 10)}$$

$$C_{norm} = C_i * k_{norm} \quad \text{(Eq. 11)}$$

After normalization, the average total concentration is within the range of the initial set up condition, ranging from 0.3% to 0.6 % (**Figure 7**). This is the final structure of a new version of the sediment concentration profile.

This finding implied that there is a problem with regard to the understanding of sediment concentration in turbidity current and the relation between bed shear stress related to the amount of sediment in suspension. It was decided here to adjust the sediment concentration

derived from the Rouse Equation in such a crude ad hoc manner because we are more confident about the structure of turbidity current, the relation between the amount of sediment concentration and the bed shear stress, but less confidence in the accuracy of the Rouse Equation in modeling suspended sediment.

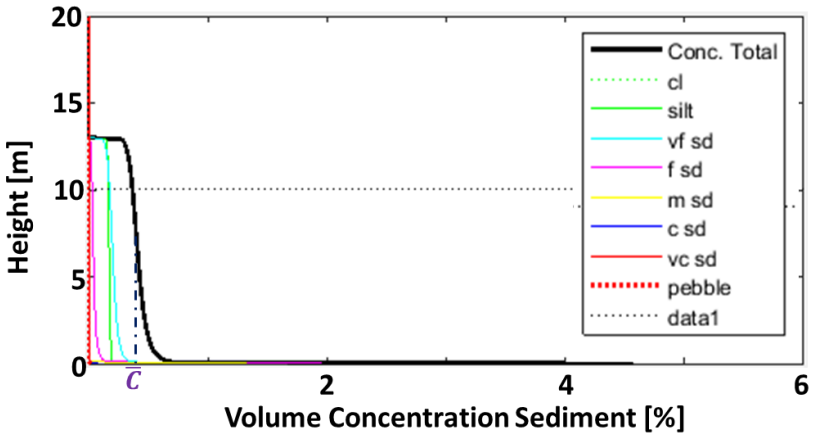

Figure 7. The sediment concentration profile obtained from the Rouse Equation after normalization. the average total sediment concentration $\bar{C}$, is 0.45 %. Data 1 in the graph represent the channel depth

2.2 Development of the SBE-Lobe

The SBE-Lobe was built through incremental steps include increasing the complexity of the model structure (**Figure 8**). It started with the simplest structure to model the settling of the grain as a function of the elevation. In this case, uniform velocity and grain-size are applied without taking into account the sediment concentration. Then, it continued by included the concentration profile and the sediment volume into the calculation, discretize the concentration profile, and uses that information to calculate the thickness distribution over the length. The next step of complexity is to put many concentration profiles for each grain-size.

2.2.1 Modeling Lobes Length and Width

The model development is started with the simplest structure and ignoring the sediment concentration. Initially, we set up uniform grain-size. So, the sediment transport distance mainly influences by the initial grain-size elevation (**Figure 8**a). Material that concentrated near the bed will be deposited in the proximal area while the one suspended high above the bed will be settling down much longer and deposited further away from the area where the channel stop. Then, we establish the well-stratified grain-size to see the influence of different particle sizes to the sediment transport distance.

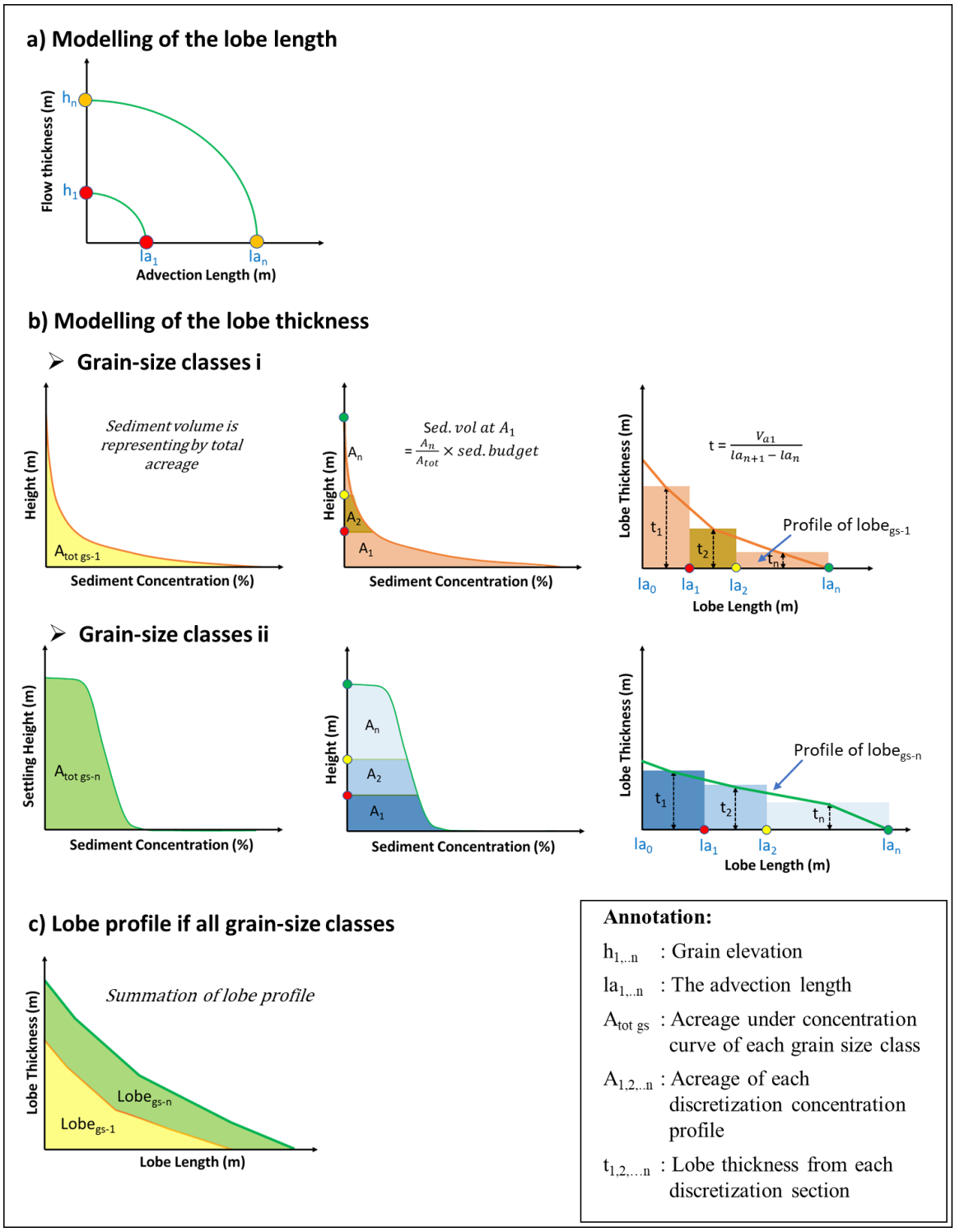

Figure 8. Schematic illustration of the SBE-Lobe model development, a) Modeling the lobe length as a function of the grain elevation, b) Modeling the lobe thickness as a function of concentration profile and the sediment budget, discretization of the sediment concentration profile, predicted advection length and lobe thickness of respective grain size classes, c) Modeling the lobe profiles

The length of the lobe is calculated using the advection length method. The advection length is a simple method to calculate the sediment transport distance of turbidity current based on the flow velocity (u), settling velocity (v_{si}) and the flow thickness (h) (Ganti et al., 2014). These three parameters assumed strongly influenced the size of turbidity current deposits (e.g., Mulder and Alexander, 2001; Ganti et al., 2014). This technique has been proved through a laboratory flume experiment that can be used as a first-order estimation tool for down-flow length, with an average of approximately 50% accuracy (Spychala et al., 2019).

In the model, we assigned a single flow velocity value for all elevation and it does not change as a function of space and reduction on the sediment concentration. The flow velocity is derived from the SBE-Channel simulation by calculating the mean velocity from the base to the top flow thickness of the Rouse equation. For the settling height, we slightly deviate from simple mathematical approximation used by Ganti et al. (2014). Instead of using a single mean value h_s, multiple elevations is assigned to grain-size class i based on the sediment stratification model (**Figure 7**), which better reflects the natural process. The settling velocity is calculated using the Eq 8 derived by Ferguson & Church (2004), as discussed in section 2.1.2. The advection length expresses as:

$$l_{ani} = \frac{u\, h_{ni}}{v_{si}} \qquad \text{(Eq. 12)}$$

Where l_{ani} is the advection length of grain-size class i from elevation n [m]; u is the flow velocity [m/s]; h_{ni} is the elevation of grain-size class i [m]; and v_{si} is the settling velocity of grain-size class i [m/s].

Figure 9 shows the result of modeling the simple structure. By assuming uniform grain size, the advection length increases linearly as a function of initial elevation. With 5 m/s flow velocity, 150 µm grain size located at 10 m above the bed is transported to 3.3 km. The gradient of advection length (l_a) also a function of grain size. The gradient of l_a decreased as a decreased grain size; coarse grain size has a high gradient while the finer grain size has a low gradient and a wider range of advection length scale. It means that changing in elevation has an enormous effect on the transport distance of fine material.

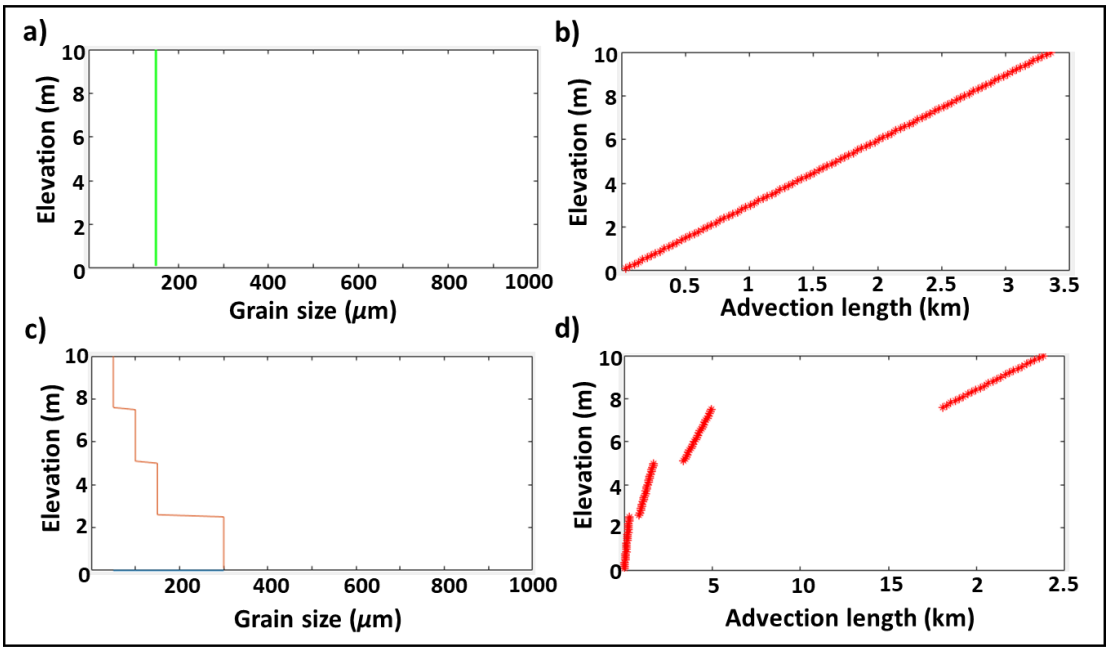

Figure 9. Development of the advection length. a) Uniform grain size, 150 µm, b) The advection length derived from uniform grain size, c) Well stratified grain size stratification, d) The advection length derived from stratified grain size. The flow velocity is 5 m/s.

This observation emphasizes Sphycala et al., (2019) argument that the advection length approach suggested simple sediment settling with the lowest and the coarsest grain deposit earlier, whereas the highest and the finest grain will transport the sediment further to the basin.

The fan lobes width is defined by setting the ratio between lobes length and width to 2:1. This simple ratio is a median value of length to width ratio discussed in various literature (E.g. Prélat et al., 2010., Pettinga et al., 2018., Spychala et al., 2019).

2.2.2 Modeling the Lobes Thickness

Another fan lobes dimension that modeled is the lobe thickness. Now, the concentration profile and the sediment volume are considered in the calculation. The lobe thickness modeling process is illustrated in **Figure 8b.**

First, we assume mass/volume balance where the total sediment budget is equal to the fan lobes volume. The total sediment budget is representing by the total area under the sediment concentration profile. Then, the area is divided into several segments horizontally. The sediment volume at each segment is calculated from the ratio of segmented area to the total acreage multiplied by total sediment budget. Afterward, we estimate the lobe thickness as a function of the amount of sediment deposited at a specified location determined from the

advection length. Eventually, the lobe profile is obtained by stacking the thickness of different grain-sizes on top of each other.

2.3 Discussion

2.3.1 The Uncertainty of Sediment Budget Estimation from the New SBE-Channel

The new version of the SBE-Channel is not only able to estimate the total sediment volume but also the sediment budget of each grain-sizes class. Thus, it can be used to calculate the rock volume of certain grain-size classes that act as a reservoir.

To test its accuracy, the sediment budget derived from the new version of SBE-Channel is compared with the result of the original SBE-Channel. The boundary condition used in the simulation is shown in **Table 2** and the simulation parameter illustrated in ***Appendix 1***. The result indicates that the new version gives a higher value in P50 estimation, 5 x 10^5 m^3 against 2.8 x 10^5 m^3. It is also giving more considerable variability as well (**Figure 10**). The variability is defined from the ratio of P90 and P10 sediment budget estimation. The new model produces P90 which is about 7.5 times higher than P10 estimation, 12 x 10^5 $m^{3,}$ and 1.6 x 10^5 m^3 respectively. While in the initial SBE-Channel the P90 (5 x 10^5 m^3) estimation is only 3.3-fold higher than the P10 estimation (1.5 x 10^5 m^3).

Table 2. Simulation Condition for Model Development

Parameters	Symbol	Value
Dynamic flow properties		
Channel width [m]	W	300 - 430
Channel depth [m]	D	10 - 10.01
Bank Angles [degree]	Bank Angles	13
Slope [Degree]	S	1.5 - 2
Initial sediment concentration [%]	Cin	0.3 - 0.6
Grain size for 50th and 90th	d50 ; d90	d50: 1.84 x 10-4 d90: 3.49 x 10-4
Maximum sediment concentration [-]	Cmax	0.585
Flow duration properties		
Turbidity current duration [hrs]	CurDur	3 - 6
Frequency of turbidity current [-]	CurFreq	0.01 - 0.0101
geological system activity [kyr]	SysAct	0.1 - 0.101

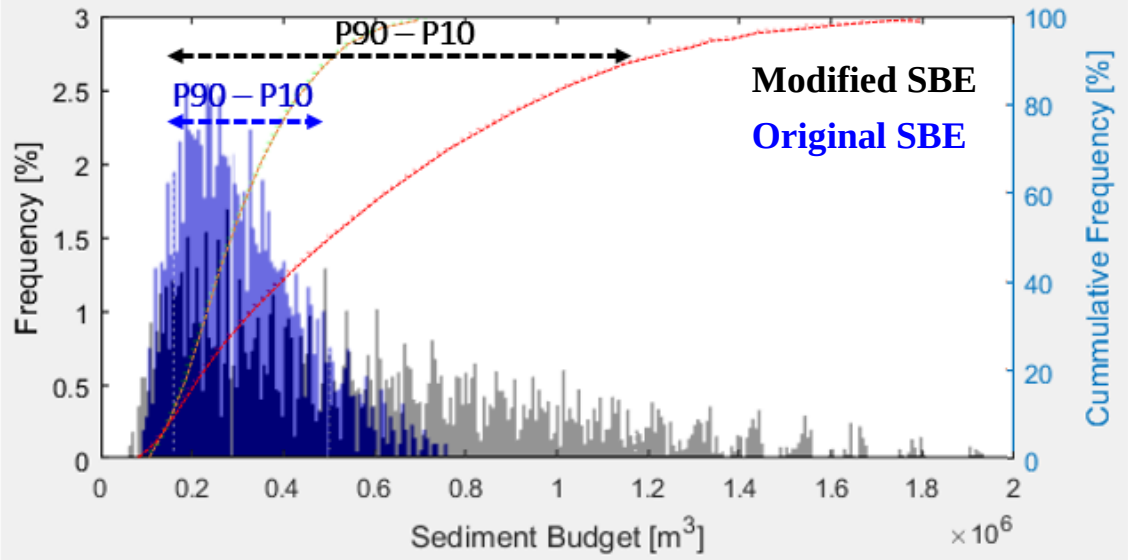

Figure 10. Comparison of sediment budget estimation from original SBE and modified SBE. P10, P50, and P90 sediment budget estimation form original SBE are 1.5 x 10^5 m^3, 2.8 x 10^5 m^3, 5 x 10^5 m^3, and from modified SBE are 1.6 x 10^5 m^3, 5 x 10^5 m^3, 11 x 10^5 m^3. Orange and red dash line is the cumulative frequency of original SBE-Channel and modified SBE-Channel.

This can be explained by the fact that we applied a different equation for generating the sediment concentration structure. The exponential decay equation produces a very well stratified single concentration profile. Whereas, the Rouse approach delivers multiple concentration profiles representing each grain-sizes class; the coarse sediments have a stratified profile, but fine material has less stratified and relatively homogenous concentration (**Figure 11**). In the original version, the maximum flow velocity lies in low sediment concentration, but in the new version, it lies on the elevation where silt and very fine sand grain class have a high concentration (**Figure 11**). It is resulting in a higher range of sediment flux, which leads to a higher range of sediment budget estimation.

Based on Eggenhuisen et al. (2019b) the Rouse Equation is an accurate model of the concentration profile of the coarsest sediment that mostly suspended at the base of the flow, but over-predicted sediment concentration for the fine-grained particle, particularly at the top of the flow. The different conditions of turbulence diffusivity between the open channel and the turbidity current possibly caused this error (Eggenhuisen, 2019b). So, even though the Rouse approach is based on the physical process of sediment concentration, applying the Rouse equation in a turbidity system to generate the sediment concentration profile delivers a high range of prediction uncertainty, especially for the fine-grained sediment.

From the perspective of petrography analysis, a typical degree of confidence in recognizing the grain size under the microscope is 50 µm. It is implied that the fine grain size cannot be recognized very well in the thin section, and it is also problematic to model it with the Rouse Equation. Therefore, it considers disregarding the sediment volume from the silt and clay grain size class.

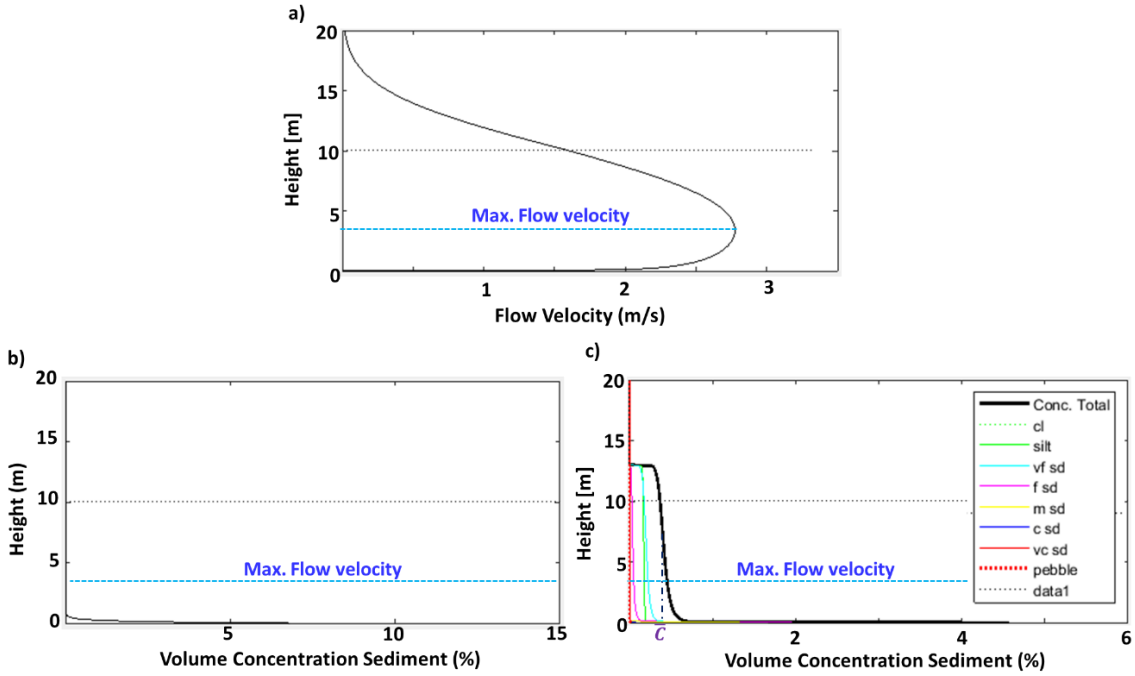

Figure 11. Flow dynamic of simulation. a) Velocity structure, b) Sediments concentration profile from the initial SBE-Channel and, c) Sediment concentration profile from the new version of SBE-Channel

By ignoring the volume fine grain particle (silt and clay particle), the new SBE-Channel produces a relatively similar value of P50 estimation in comparison to the original SBE, 2.9 x 10^5 $m^{3,}$ and 2.8 x 10^5 m^3 correspondingly (**Figure 12)**. So, it clear that application the Rouse Equation in the turbidity current has a problem with modeling silt and clay.

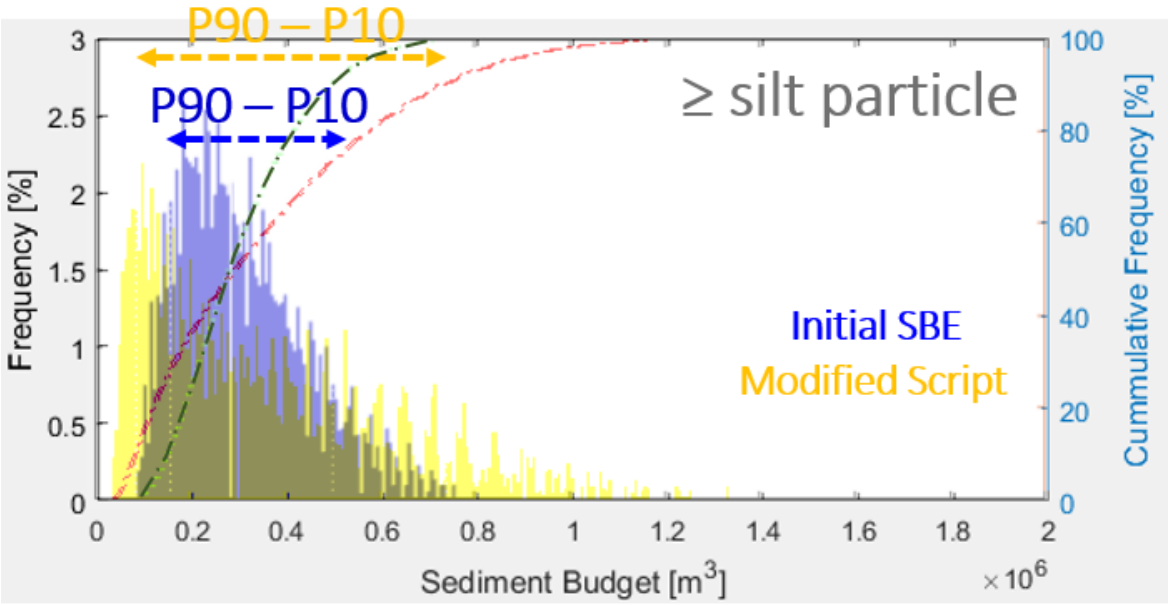

Figure 12. Comparison of sediment budget estimation from original SBE and modified SBE for particle higher than silt. Orange and red dash line is the cumulative frequency of original SBE and modified SBE. The Green and red dash line is the cumulative frequency of original SBE and modified SBE.

2.3.2 Sensitivity Analysis of Sediment Budget Estimation

Since the variability of sediment budget estimation of the new SBE-Channel is higher, here we present the sensitivity analysis for different simulation conditions to evaluate which factor has a critical impact on the uncertainty by varying one by one the simulation variables by +20% and -20% relative to the base case (**Figure 13**). The variability is defined from the range of P90 and P10 sediment budget estimation.

It indicates that low variability in defining simulation conditions results in a low sediment budget estimation range. The highest contribution to the uncertainty is channel geometry, followed by initial concentration and current duration, while slope has relatively insignificant on the uncertainty. It means that a better understanding of the geological condition will lead to better accuracy in the modeling of that system.

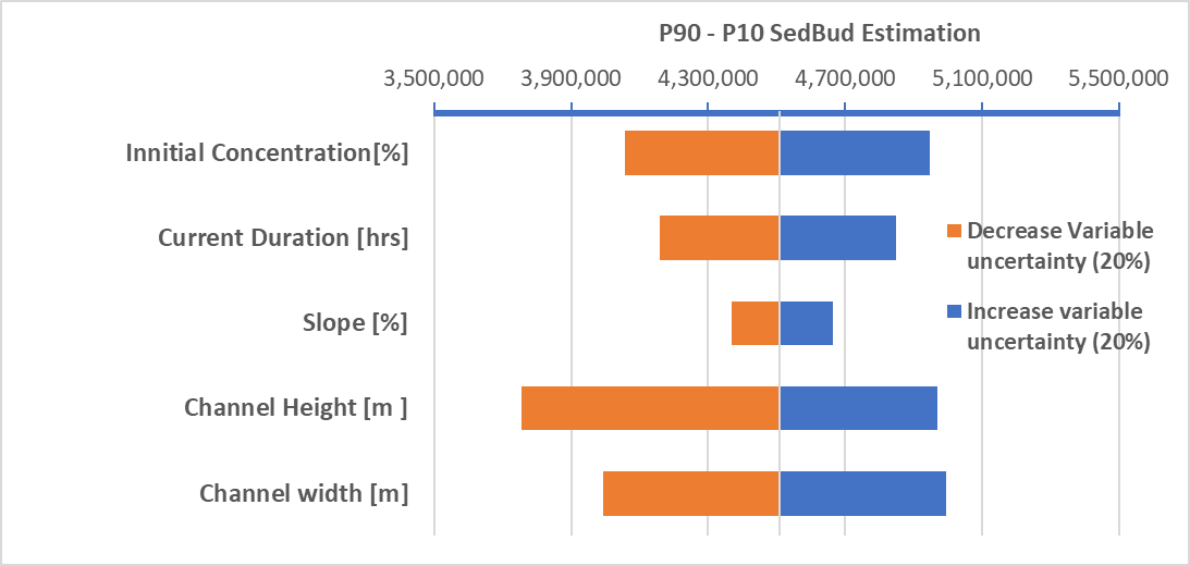

Figure 13. Sensitivity analysis of simulation variables to the new version of SBE-Channel. The variability is defined from the range of P90 and P10 sediment budget estimation. The base case and the parameter value are shown in **Appendix 2.** Variables used in the sensitivity analysis in the section 2.2.3

2.3.3 Level of Hierarchy

The proper level of hierarchy needs to be established when developing the prediction model (Hamilton et al., 2017). We realize that lobes are comprised of stacked lobe elements and the lobe elements are built from several beds (Deptuck et al., 2008; Prélat et al., 2009; Prélat et al., 2010; Grundvåg et al., 2014; Spychala et al., 2017a,b; see **Figure 14**). The complexities of the lobe cannot be modeled by the current version of the SBE-Lobe yet.

However, the rate of compensation stacking decreases with lower hierarchical levels (Straub and Pyles, 2012). The fact that lobe elements can be interpreted in the field from the similarity of bed facies that made up them (e.g. Prélat et al., 2009; Prélat and Hodgson, 2013) confirm the assumption that the depositional setting might remain stable during their deposition. Therefore, we propose that the model can be compared against the bed and lobe element geometries that comprise of weakly compensational beds.

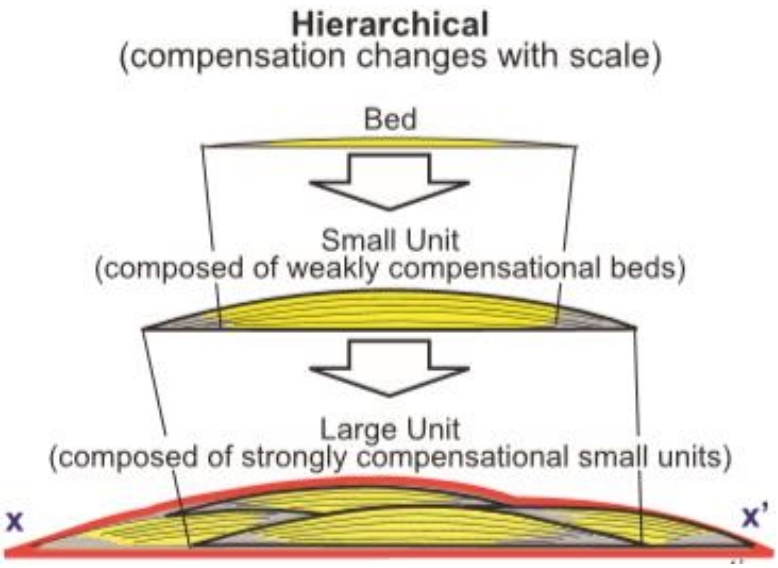

Figure 14. Lobe Hierarchy Diagram, large units more compensational that small units (from Straub and Pyles, 2012)

3 Model Validation

The validation process is necessary to check the accuracy of the simplified model in predicting fan lobes geometry. We validate the model with the run-5 flume experiment performed by de Leeuw et al. (2018). Detailed experimental setup and procedure used during the experiment are described in de Leeuw et al. (2018). We organized the same setup boundary condition as the simulation variables (such as the channel geometry, slope, initial sediment concentration, and flow duration) and examine which aspect of the lobe type can be predicted by the simplified model.

3.1.The Boundary Condition and the Result of Flume Experiment

The boundary conditions used in a run-5 flume experiment are shown in **Table 3.**

Table 3. The boundary condition of the flume experiment (de Leeuw et al., 2018)

Boundary Conditions	Symbol	Value
Suspension tank volume [L]	-	900
Initial sediment concentration [% vol.]	Cin	17
Discharge [L/s]	SedFlux	8.3
Slope angle [^{0}]	S	11
Basin-floor angle [^{0}]	-	0
Flow duration [s]	Flowdur	92
Channel width [m]	W	0.8
Channel depth [m]	D	0.03

From the experiment, most of the sediment is deposited in the basin floor, formed fan lobe body with the depocenter located about 1 meter from the end of the channel. The forming lobe demonstrates that the sediment is thinning laterally and longitudinally. The length and width of the main lobe body that formed are about 2.6 m and 1.3 m respectively.

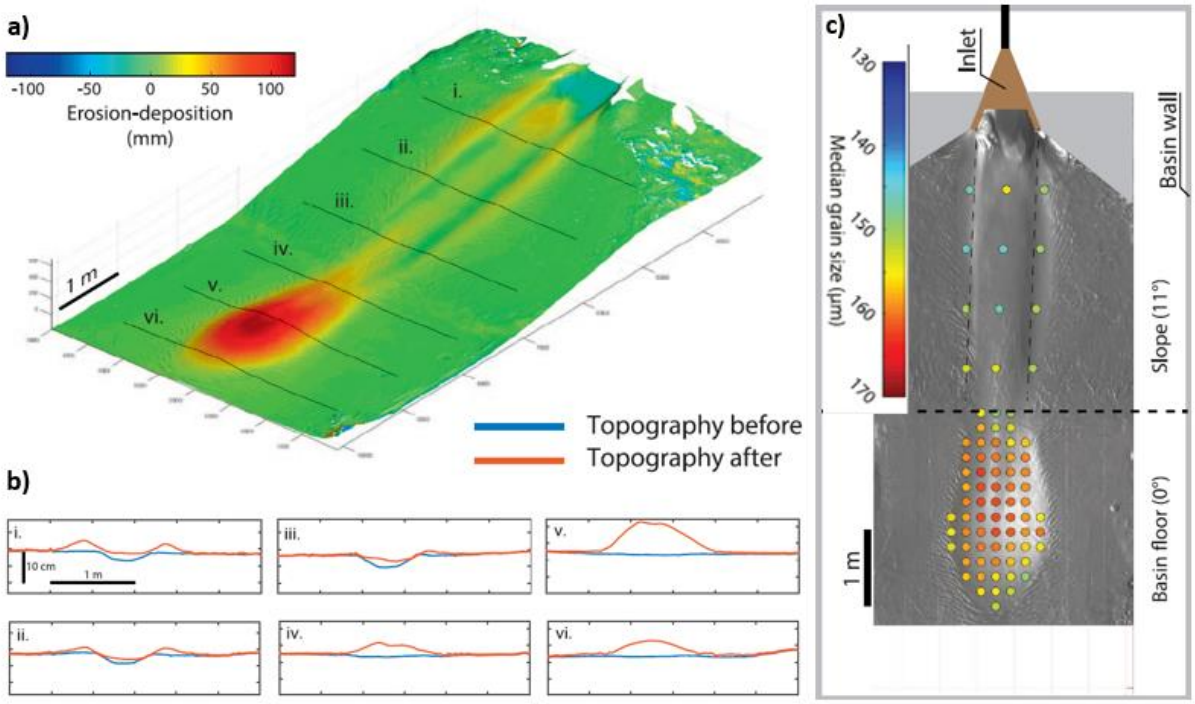

Figure 15. The experiment result of run 5 a) Maps of deposition and erosion with respective cross-sections, b) Cross-section of channel and lobe, c) Median grain size of deposited sediment. Star is the sample location that used as an input in simulation (Figure is adopted from de Leeuw et al., 2018 with certain modification)

For the grain size analysis, de Leeuw et al., (2018) sampled the deposits from the slope and the basin floor deposit in a regularly spaced sampling grid (**Figure 15**). These samples were analyzed using a laser particle-size analyzer (Malvern 2000 Mastersizer) which is grouped the grain-size with bin width 0.16 ϕ. These data have to be adjusted into 0.25 ϕ bin size prior utilized it in the modeling. The process is accomplished by rearranging the grain size distribution data into new pre-defined groups.

The grain size distribution data from one channel deposits (marked with a star in **Figure 15c**) are used for the input in the simulation (**Figure 16**). Meanwhile, the grain size distribution data from lobe deposits are used for model validation.

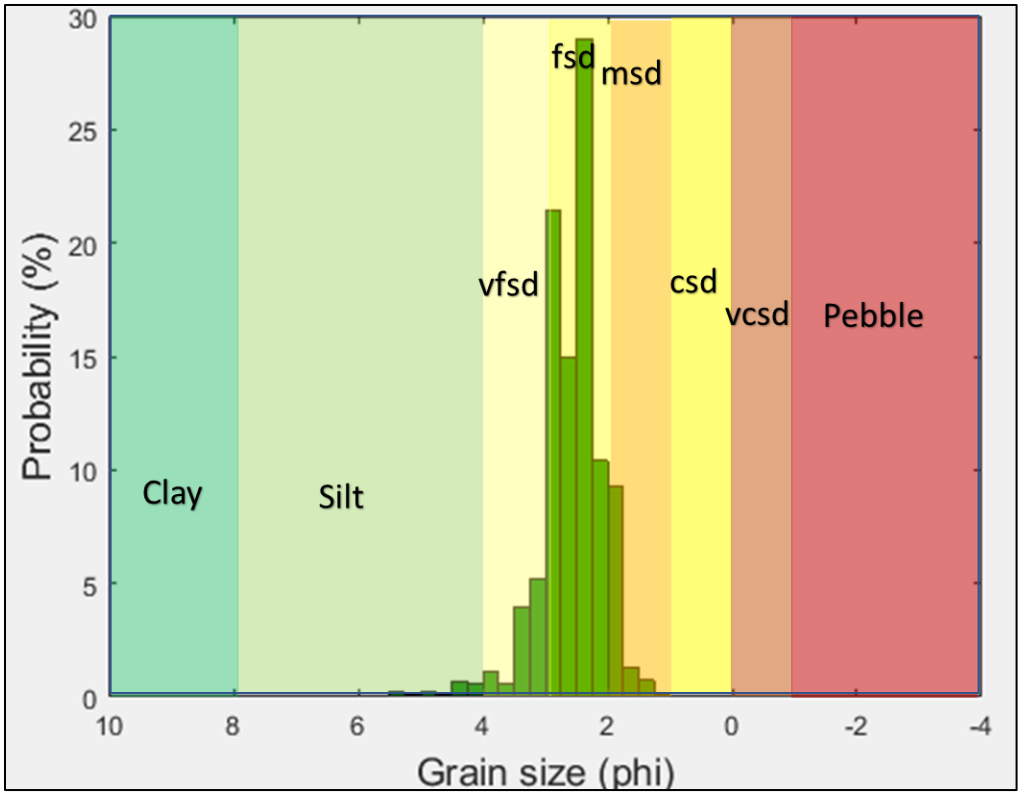

Figure 16. The grain size distribution of channel deposits for the input data in simulation. Sample location mark as a star in Figure 14. The grain size range is referred to the Table 1

The predicted lobe model of a run-5 flume experiment is shown in **Figure 17**. The predicted model shows a simple wedge sediment body with the most substantial volume sediment located close to the slope break and thinning downward. The sediment layer presented in the model is not representing the vertical sequence of deposition but expresses the relative portion of that grain size in a certain position. Referring to the sub-marine environment classification (Prélat et al., 2009; Prélat and Hodgson, 2013; Kane et al., 2017), the resulting model can be grouped into lobe axis – lobe off-axis, lobe fringe and distal lobe fringe based on lobe thickness and the grain size content. Lobe fringe deposits are characterized by abrupt lateral changes in thickness and these facies consist of very-fine grain sand. In the model, the lobe axis and lobe off-axis appear in the same area because the cross-section is the representation of the full width of the fan lobes.

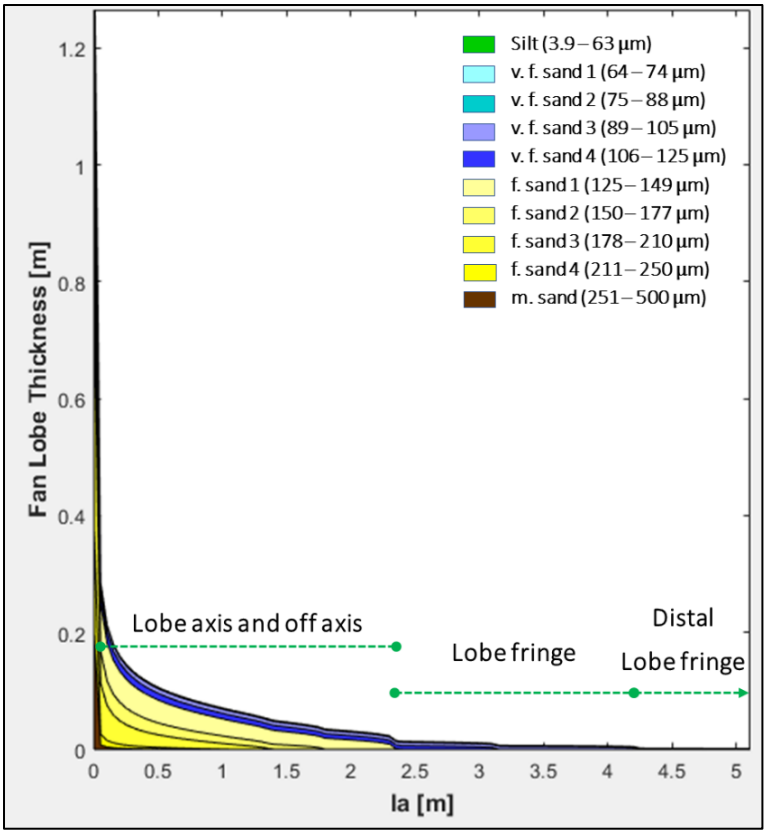

Figure 17. The predicted fan lobe model of run-5 flume experiment

3.2 Evaluation of Lobe Geometry from Model

The length of the lobe axis and lobe off-axis from the model, on the first inspection, give the result within the amplitude of the fan lobe of the experiment (**Figure 15a**). However, significant thickness discrepancies are observed in the lobe apex. Additionally, we also verify the accuracy of modified SBE in regard to the sediment budget estimation.

3.2.1 Sediment Transport Distance

In the model, sediments are deposited in the area between the slope break and its maximum advection length. The maximum advection length of each grain-grain size class then being compared with the maximum transport distance of sediment from the experiment (**Table 4**) to evaluate the model accuracy in predicting the lobe length. Due to the limitation of the flume length used in the experiment, the sediment with advection length higher than 11 m, such as silt particles, cannot be validated

Table 4. Comparison of sediment transport distance of different particles size between model and experiment

Grain Size		Transport Distance (m)
Silt (< 0.063 mm)	Model	116
	Experiment	nd
v.f. sand1 (0.063 - 0.074 mm)	Model	7.98
	Experiment	2.67
v.f. sand2 (0.075 - 0.088 mm)	Model	5.8
	Experiment	2.67
v.f. sand3 (0.089 - 0.105 mm)	Model	4.26
	Experiment	2.67
v.f. sand4 (0.106 - 0.125 mm)	Model	3.15
	Experiment	2.67
f. sand1 (0.126 - 0.149 mm)	Model	2.35
	Experiment	2.67
f. sand2 (0.15 - 0.177 mm)	Model	1.78
	Experiment	2.67
f. sand3 (0.178 - 0.210 mm)	Model	1.37
	Experiment	2.67
f. sand4 (0.211 - 0.250 mm)	Model	1.06
	Experiment	2.67
m. sand (0.251 - 0.500 mm)	Model	0.55
	Experiment	2.67
c. sand (0.501 - 1 mm)	Model	0.29*
	Experiment	2.67
pebble (0 > 2 mm)	Model	0.1*
	Experiment	2.67
50 % to 60 % prediction accuracy		
60 % to 80 % and 121 – 160% prediction accuracy		
80 - 120 % prediction accuracy		

* only based on a calculation

The comparison suggests that the model can predict the sediment transport distance of very fine sand to fine sand (0.089 – 0.210 mm) particle sizes. The best prediction accuracy is at 0.106 to 0.149 mm grain size class, with higher than 80% accuracy (highlight in green). Followed by the 0.089 to 0.105 mm and 0.15 to 0.177 grain size class with 60 % - 80 % prediction accuracy (highlight in blue), and the 0.178 to 0.210 mm grain size class has 50 % to 60 % prediction accuracy (highlight in yellow).

However, the model underpredicted the sediment transport distance of the coarser particle (> 0.211 mm) and over predicted the sediment transport distance of fine particles. The simplified model drops the coarse particle too quickly; the sediment is rapidly depleted, which is not represent the lobe geometry from the experiment.

3.2.2 Lobe Thickness

On the first inspection, the length of the lobe axis and lobe off-axis from the model is within the amplitude of the fan lobe of the experiment. But the predicted model shows the most substantial volume sediment located close to the slope break (**Figure 17**). Differently, the lobe obtained from the experiment has a mounded geometry where the main depocenter located about 1/3 of the length of the main lobe body (**Figure 18**).

In more detail, the comparison between the predicted model and the experiment result is shown in (**Table 5**). Although the model is significantly overestimated the thickness of the lobe in the proximal area (highlight in red), the model produces better lobe thickness prediction for the middle and the distal area. This finding suggests that the model can be used as the first-order estimation of lobe thickness in the middle and the distal area, but it cannot model the apex lobe geometry. This finding emphasizes the Spychala, Y.T et al., (2019) hypothesis, that the advection length method is unable to predict the main depocenter of deposition because of the thickest deposition in an advection model is always located at the channel mouth.

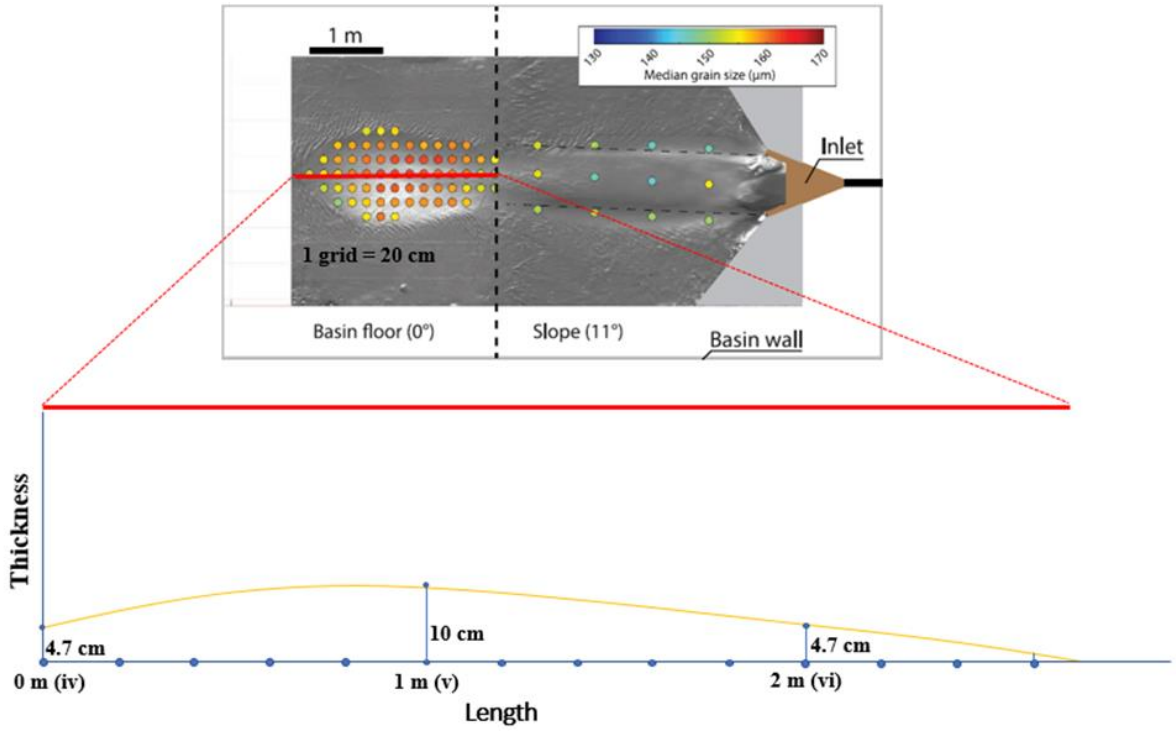

Figure 18. Maps with a median grain size of deposit samples collected and the illustration of run-5 lobe thickness with twice vertical exaggeration. The blue dots on the cross-section represent the sampling point location. The letter (iv, v and vi) are indicating the location that intersects with the cross-sections shown in **Figure 15b** (modified from de Leeuw et al., 2018)

Table 5. Comparison of lobe thickness from the model and the experiment at 20 cm interval. Red highlight is representing the area where the model overestimated the lobe thickness

Distance from channel	Fan Thickness (cm)		
	Experiment	**Model**	**Ratio**
0	4.7	163.26	3474%
20	6.65	19.85	299%
40	8.3	14.34	173%
60	9.25	11.57	125%
80	10	9.68	97%
100	10	8.18	82%
120	9	6.87	76%
140	8	5.37	67%
160	7	4.69	67%
180	6	3.55	59%
200	4.7	3.16	67%
220	3.75	2.65	71%
240	2.75	1.14	42%
260	1.15	1.08	94%

3.2.3 Spatial Grain-Size Distribution within the Lobe

The spatial grain size distribution within the predicted lobe geometry is compared to the experimental grain size distribution through three steps. First, re-grouping the grain size distribution data from the experiment into 0.25 ϕ bin width. Then, make the average grain size distribution of all samples on the lobe deposits at a given distance. Next, calculating the grain size fraction of predicted lobe at the same location as the experiment sampling points and evaluate the result (**Figure 19**).

The spatial grain size distribution obtained from the predicted model and the experiment, in some area, shows the relatively same pattern. Both models and experiments indicate that about half of the lobe length, the lobe is dominated by the fine sand particles. It also can be seen that the model can spatially predict the deposition location of fine sand1 and fine sand2 grain class. However, the modeling result predicts the coarse particles depleted too quickly from the turbidity current. It implies that the average grain size distribution at the distal area derived from the model is questionable.

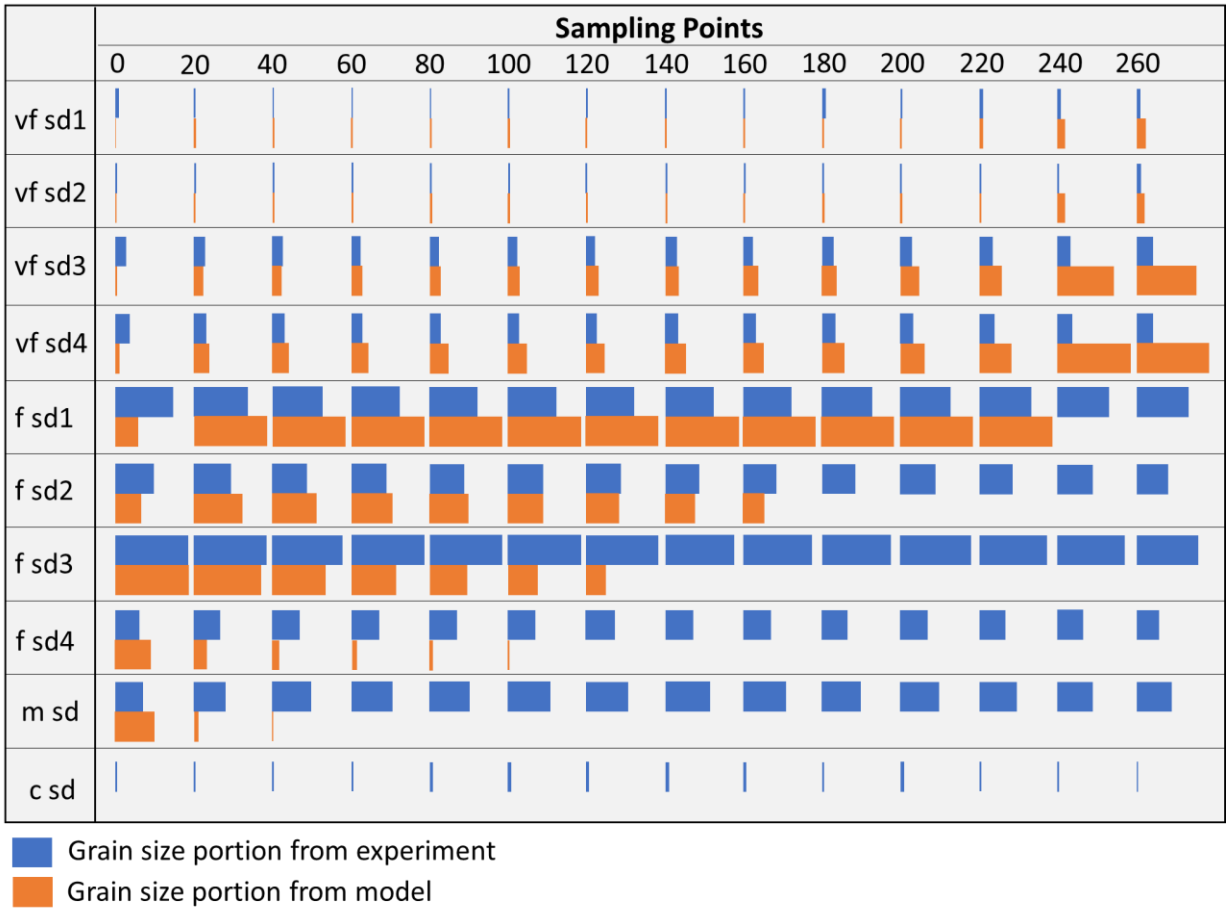

Figure 19. Comparison of spatial grain size distribution between lobe from the experiment and the predicted model. The bar represents the grain size distribution at a sampling location.

3.2.4 Sediment Budget Estimation

The sediment budget of the flume experiment has been estimated through the new SBE-Channel and the initial SBE-Channel, the result for P50 estimation is 0.342 m^3 and 0.255 m^3 respectively (**Table 6**). Meanwhile, the actual sediment budget of a run-5 experiment is 0.13 m^3. This means that the former provides an estimation of 2.6 times higher than the actual sediment budget, while the latter is 2 times higher.

This result reinforces the previous finding that the new SBE-Channel appears to over-predict the sediment budget. However, this validation shows that the model is successful in predicting the sediment budgets in a factor of 2-3.

Table 6. Comparison of actual sediment budget and estimated sediment budget using modified SBE and initial SBE

	P10	P50	P90
Actual SedBud [m^3]		0.129	
Modified SBE			
Total SedBud [m^3]	0.335	0.342	0.35
> v.f sand particle [m^3]	0.275	0.281	0.287
Initial SBE [m^3]	0.249	0.255	0.26

3.3 Validation Result and Discusiion

Model validation has revealed the advantages and limitations of the SBE-Lobe module. Construction of sediment concentration profile using the Rouse Equation for all grain size ranges allows us to develop the fan lobe geometry prediction tool. This tool gives a fairly accurate lobe thickness in the middle and the distal area (**Table 5**). Furthermore, it also can locate the area where the fine sand grain size class is mainly deposited (**Figure 19).** Since this grain size range is promising as a reservoir candidate, we propose this method can be used as the first-order prediction for reservoir distribution. One major limitation of this model is the inability to capture the thickness and grain size particle in the lobe apex or at CLTZ.

3.3.1 Sensitivity Analysis for the Advection Length Parameters

The sensitivity analysis is performed to evaluate the uncertainty of the advection length parameter and its influence on the submarine lobe geometry. The evaluation is conducted by varying one by one of the variables by +15% and -15% relative to the base case (**Figure 20** and **Figure 21**). The base case referred to the simulation condition used in the run-5 flume experiment.

The effect of the parameter uncertainty on the sediment transport distance is assessed to the fine sand1 grain class. The analysis indicates that flow thickness and the velocity influence the sediment transport distance to the same extent. An increase in the flow thickness and/or flow velocity by 15% results in an increase in the sediment transport distance by 15%. It can be explained by referring to the advection length equation **(**Eq. 12**)**, with constant settling velocity, the advection length is proportional to the flow thickness and the flow velocity. Meanwhile, the sediment budget does not impact the sediment transport distance.

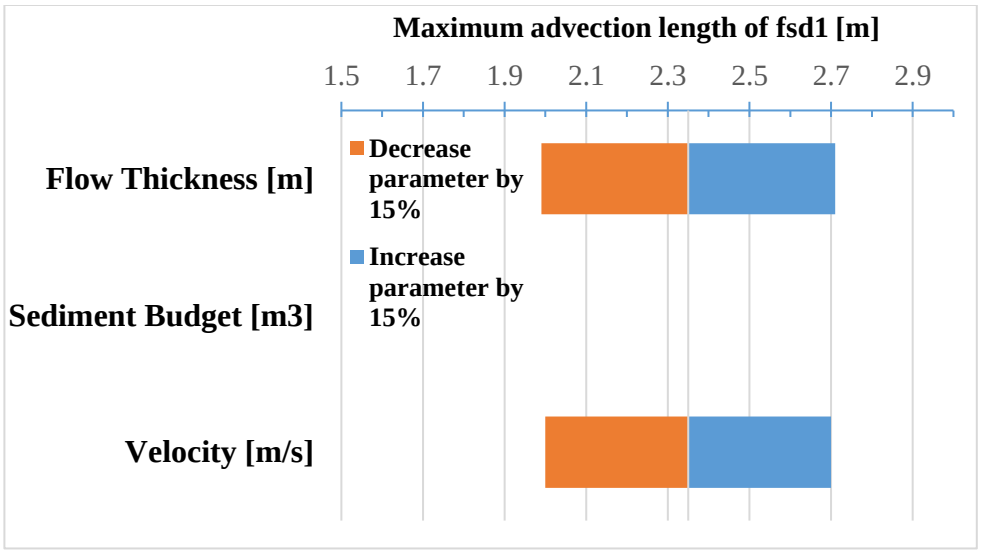

Figure 20. Sensitivity analysis of the advection length parameter to the sediment transport distance. The base case is 2.35 m

Hereafter, the effect of the parameter uncertainty on the lobe thickness is observed at 1 m from the base of the slope. The evaluation shows that changing in all three parameters affect the lobe thickness with the main contribution is the velocity. An increase in the velocity and flow thickness is followed by a decrease in the lobe thickness. This happens because the faster flows carry sediment further, hence formed thinned beds. On the other hand, an increase in the sediment budget creates a thicker lobe profile.

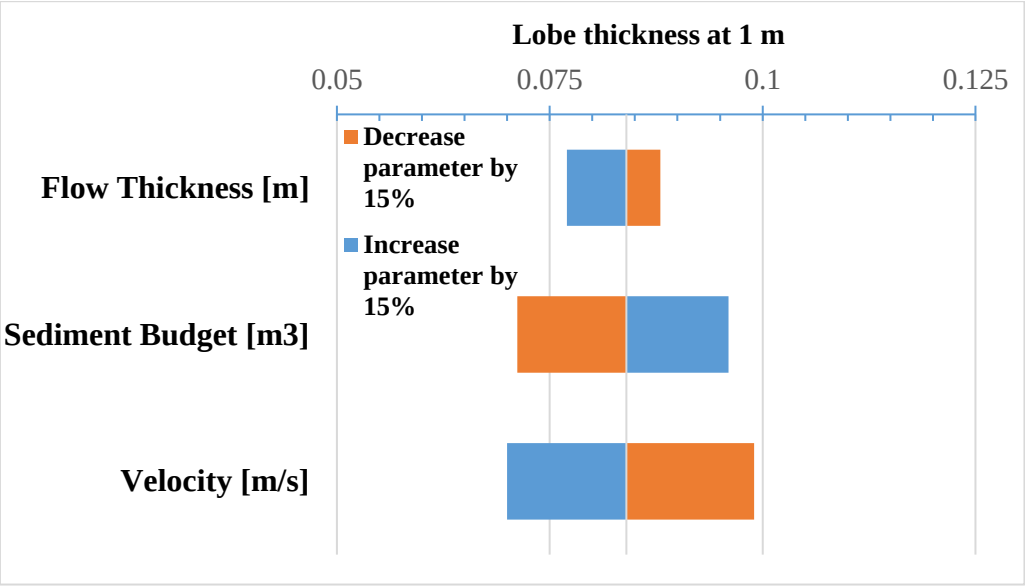

Figure 21. Sensitivity analysis of the advection length parameter to the lobe thickness. The base case is 0.084 m

3.3.2 Model Limitation

Besides the uncertainty in determining the sediment budget estimation, there are several assumptions and simplifications applied in the model development that might be contributed to the model accuracy. The advection length method used in this study has not accommodated the mechanism occurring in the CLTZ. The CLTZ is the area within the turbidite systems where the flows experience rapid expansion because of abrupt changes in the gradient and a decrease in confinement (Mutti and Normark, 1987). The zone that separates well-defined channels from the lobes is dominated by sediment bypass process, deposition, erosion, and turbulence production that influence the facies distributions and the depositional architecture.

Ignoring the mechanism that occurred in the CLTZ is the main reason why the model tends to over-estimate the lobe thickness in the proximal area and under-estimate the sediment transport distance of the coarser particle. The model assumes that flows lose their confinement and deposits their sediment immediately after reaching the end of the channel. Dynamic processes that occurred on the CLTZ would keep the particle remain in the suspension and transport it further to the basin, reducing the lobe thickness in the proximal and increasing the lobe thickness in the middle and distal lobe. While some scientist hypothesize that the erosion at the CLTZ is caused by the occurrence of the hydraulic jump (e.g., Komar, P. D. 1971, Mutti, E. & Normark, W. R. 1987, Wynn, R. B., et al., 2002), Pohl, F. et al., (2019) explain this mechanism as a result of flow relaxation at the end of submarine channels.

Hansen et al. (2019) suggest that seabed architecture affects the character of basin-floor turbidity current deposits and sediment distribution. The seabed confinement constraints the facies distribution and the pattern of an individual lobe. The more confine basin floor fan the longer the lobe is formed. This aspect also does not cover by the simplified model. Moreover, the model is built by assuming no lateral thickness changes. It suggests that the lobe thickness presented by the model is the average lateral thickness.

The SBE-Lobe module assumes single advection velocity for all grain size and disregards the temporal and spatial evolution of flow velocity as a result of the reduction of the sediment concentration, which also not represents the real flow velocity condition. The velocity is the main control of uncertainty (**Figure 21**). In the physical experiment, Spychala et al. (2019) observed that advection velocity decelerates about 50% over the length of the lobe.

4 Applications of the SBE-Lobe to the Ancient Turbidite Deposits

4.1. Fan lobe geometry prediction of single turbidity event Gold Channel, TrePasos Formation, Chile

The SBE-Lobe is applied to estimate the amount of sediment flows through the ancient Gold Channel. This quantification is an update from the previous estimation performed by Novianti (2019). While Novianti (2019) calculated the sediment budget for three different grain size classes, in this study we estimate the total sediment budget. This application will also illustrate the consistency and regularity of the SBE-Lobe in estimating the sediment budget since four-grain size samples of channel deposits are available.

Four samples used in the calculation were taken by de Leeuw et al. (2018) from the axis channel deposits, which further analyzed by Novianti (2019) (***Appendix 4***). The Gold Channel deposit is one of the channel elements from the sandstone package of Tres Pasos Formation, Magallanes Basin, Chile. These deposits are well exposed at Laguna Figueroa (Macauley and Hubbard, 2013). Unfortunately, the down-dip deposits of the Gold channel system that can be used to validate the predicted lobe geometry are not exposed.

The boundary conditions applied in the simulation are shown in **Table 7**. This condition is taken from the previous study performed by Novianti (2019). The calculated sediment budget of the Gold Channel derived from four different samples give relatively the same result. This indicates that the SBE-Lobe module has good regularity in predicting the sediment budget. Furthermore, this result can be a reference in determining the number of samples for estimating the sediment budget using the SBE-Lobe.

By assuming that there are 200 to 800 turbidity currents, the average sediment budget estimation for the all-grain class is 9.3×10^7 m^3, with about half of the sediment volume, 4.9×10^7 m^3, is a sand particle (**Figure 22**). The sediment budget for the sand particle is counted because the SBE-Lobe produces better estimation for higher than silt grain size class and to show the application of this module to predict the rock volume that can act as a reservoir.

Table 7. Boundary condition used to estimate the sediment budget and to develop the geometry prediction of Gold Channel deposits and Lobe 5, Fan 3 of Skoortersberg Formation

Parameters	Symbol	Gold Channel	Lobe 5
Dynamic flow properties			
Channel width [m]	W	300 - 430	450 - 500
Channel depth [m]	D	7 - 7.01	6 - 8
Bank Angles [degree]	BankAngles	13	20; 13
Slope [Degree]	S	1.5 - 2	1.5 - 2
Initial sediment concentration [%]	Cin	0.3 - 0.6	0.3 - 0.6
Grain size for 50th and 90th	d50 ; d90	d50: 1.84 x 10-4 d90: 3.49 x 10-4	d50: 2.24 x 10-4 d90: 3.97 x 10-4
Maximum sediment concentration [-]	Cmax	0.585	0.585
Flow duration properties			
Turbidity current duration [hrs]	CurDur	3 - 6	3 - 6
Frequency of turbidity current [-]	CurFreq	0.1 - 0.2*	1 and 10
Geological system activity [kyr]	SysAct	2 - 4*	0.001 - 0.00101

* For lobe geometry prediction, the frequency of turbidity current and geological system activity is setting up for modeling 1 turbidity current

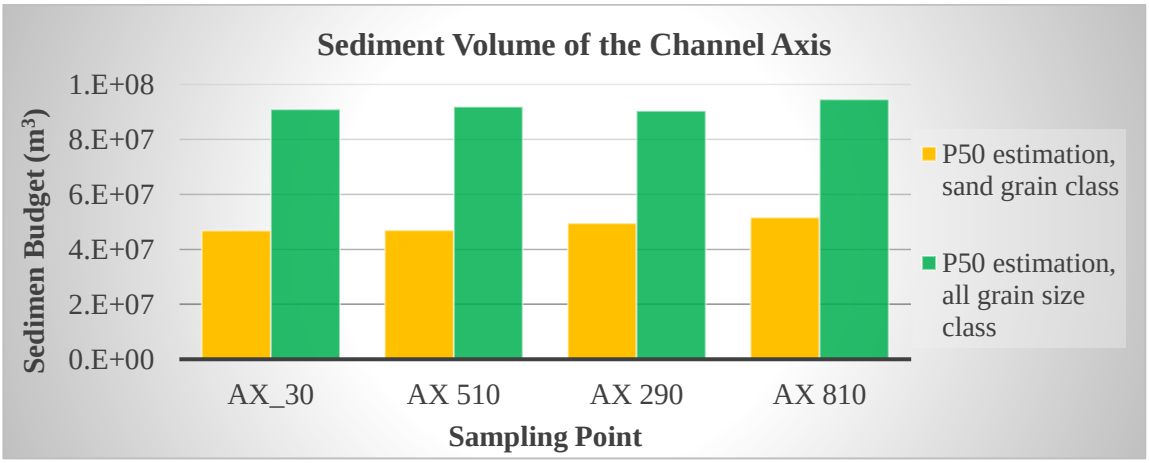

Figure 22. Sediment budget estimation of Gold Channel Deposit for all grain size classes and sand particles

For the lobe geometry prediction, the simulation condition used to calculate the sediment volume is modified to model 1 turbidity event. It is predicted that one turbidity current that flows through the gold channel system formed a lobe that dominated by very fine sand material (**Figure 23**). The fine sand class could deposit up to 870 m, very fine sand class up to 2940 m, and silt particles spread out to 43 km. The fine sand particle is thinning toward the basin, while the very fine sand relatively has homogeneous thickness. The average thickness of the middle lobe deposit is ranging from 4 to 10 cm.

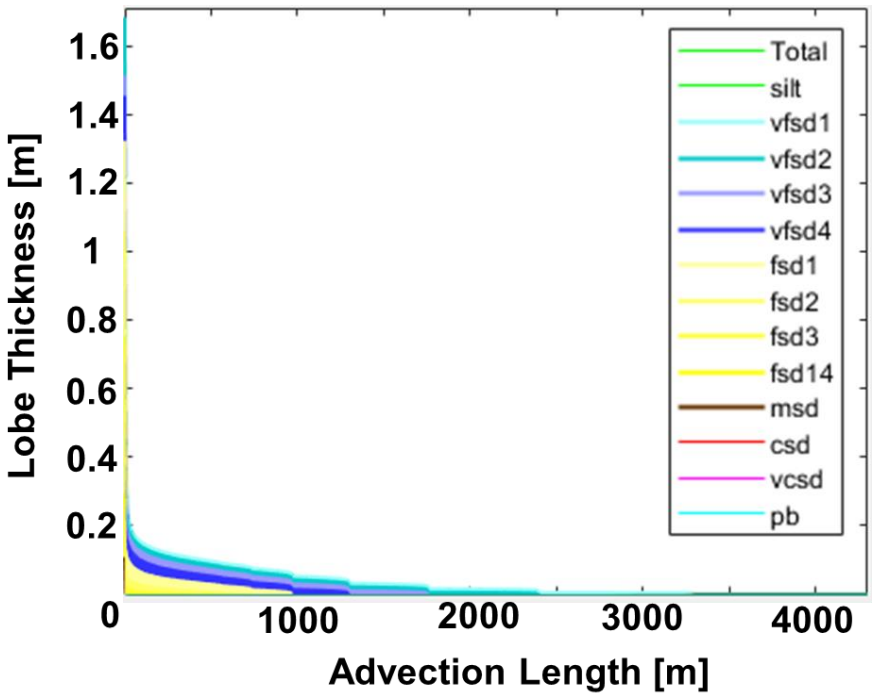

Figure 23. The predicted fan lobe geometry of 1 turbidity current flow through Gold Channel system

4.2. Fan lobe geometry prediction of lobe 5, Fan 3, Skoorsteenberg Formation, Karoo Basin, South Africa

Fan 3 of Skoorsteenberg Formation is part of the marine Ecca Group that deposited during the Permian in the Tanqua depocentre, Karoo Basin, South Africa (Smith, 1990; King et al., 2009). The lobes of Fan 3 may collectively be considered as a lobe-complex set consisting of six lobes (namely lobe 1 to 6). Each lobe is isolated vertically by fine-grained elements, called interlobes, that denote extensive sand supply reduction to the area of the lobe complex (Prélat et al., 2009). This study is focused on the reconstruction of Lobe-5.

Several field studies in the Tanqua depocenter define the stratigraphic framework of Fan 3. Kane et al. (2017) have collected and analyzed a series of data sets to study the stratigraphic record of Fan 3. These data sets, which consist of the sedimentological logs from 20 sites (scale 1:20 and scale 1:2), stratigraphic correlation, lithology, paleocurrent direction (**Figure 24**), are utilized in this study as a comparison of the predicted lobe geometry. By doing this, we can suggest the length of Lobe-5 and how many turbidity current deposit that constructed their thickness. This information is difficult to identify in the field due to the limitation of the outcrop and sand amalgamation.

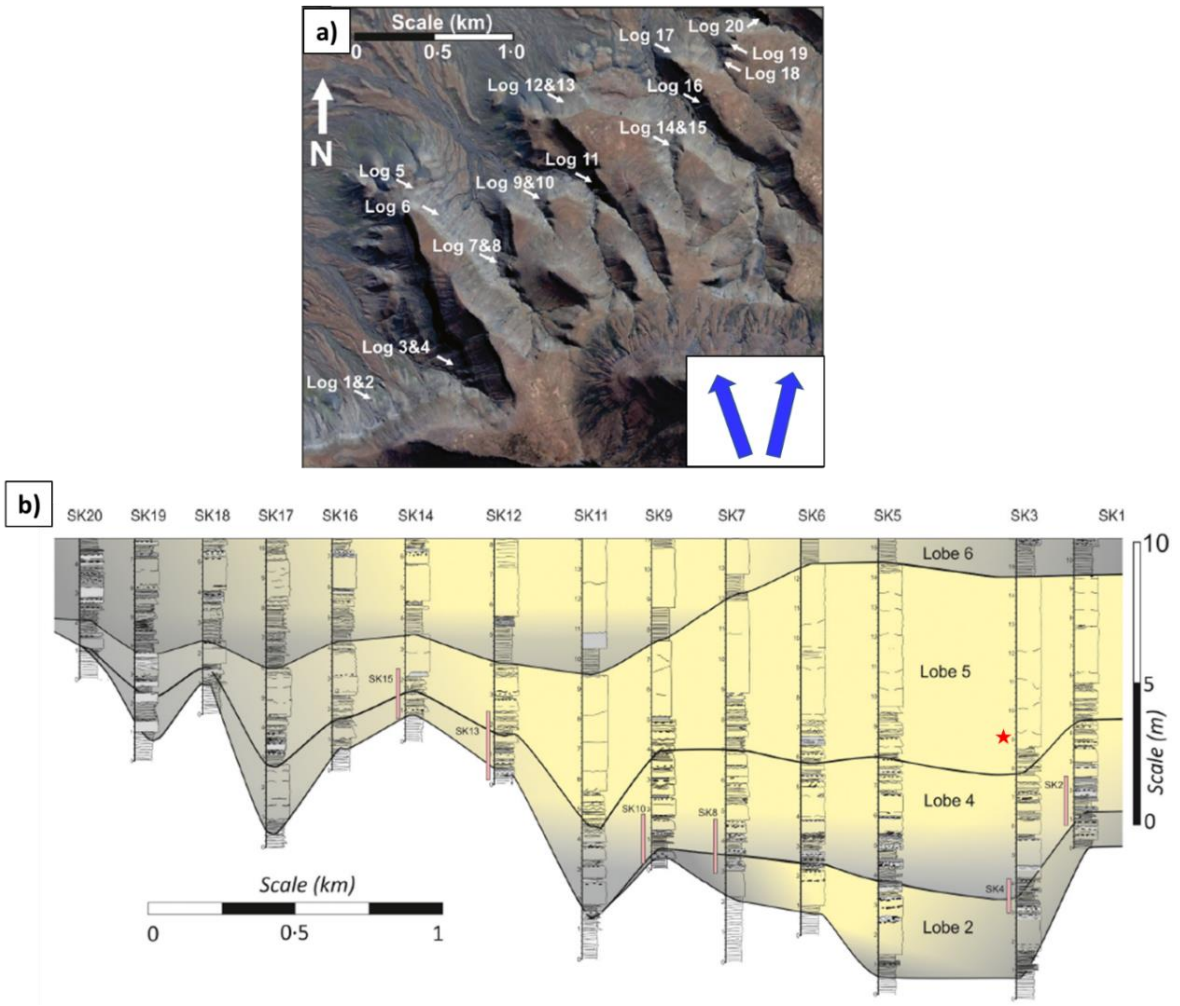

Figure 24. a) Aerial image of the Tanqua Depocenter area and the location of the measured sections. Blue arrows indicate the paleocurrent direction. b) Stratigraphic correlation of outcrop logs SK1 to SK20 (scale 1:20). The lobes stack to form a lobe complex (Fan 3). Star represents the sample location of the grain size distribution analysis data used in this study. (modified from Kane et al., 2019).

Lobe-5 thickness is ranging from 6 m in the proximal and 1 m in the distal area (**Figure 24b**). The massive sands in the Lobe-5 are thought to be amalgamated sandstones that were deposited by multiple turbidity currents. The Lobe-5 is formed from a stack of lobe elements (Prélat et al., 2009). From the correlation, lobe element thickness is ranging from 0.2 to 2.6 m, and bed thickness is ranging from 0.01 to 0.25 m. The lobe element thickness is measured from a 1:20 log scale while the bed thickness is defined from a 1:2 log scale (**Figure 25**).

With regards to the lobe length, the minimum length of Lobe-5 is 2.5 km and all-grain size classes (silt to fine sand) can be found along the cross-section. However, it must be noted that the actual length of Lobe-5 is unknown because the location where the lobe-5 is started to

form is not mentioned in the available literature. The deposition of the Lobe-5 package might also continue further to the basin. In the simulation, log SK-1 is assumed as the starting reference point.

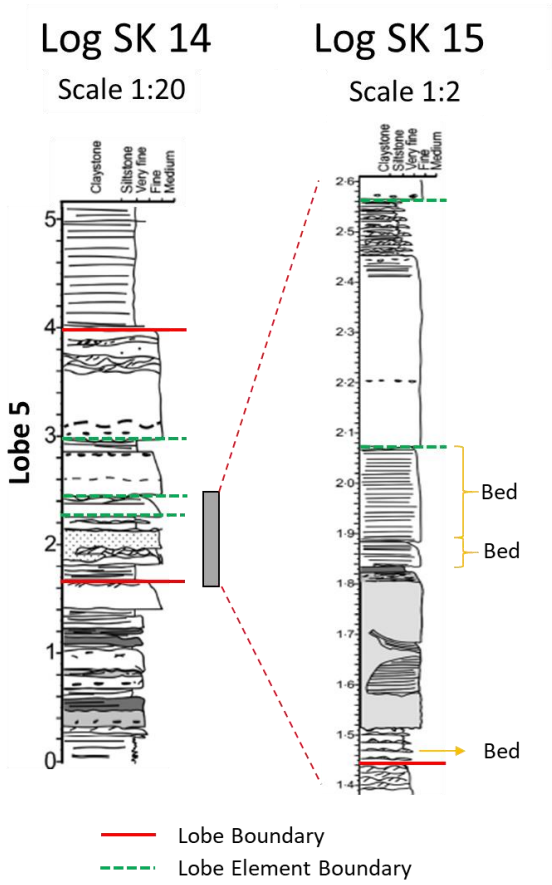

Figure 25. Illustration of how to determine the lobe element and bed thickness of Lobe-5 from log SK14 and SK15. The log location showed in **Figure 24a**. Lobe boundaries are defined in Kane et al (2017), while lobe elements and beds are interpreted in this study (Log are taken from Kane et al., 2017)

The boundary conditions required for the simulation are synthesized from various literature (**Table 7**). A channel width, 450 – 500 m, is defined from the channel fill outcrop of Fan 3 (Morris et al., 2000). Channel depth is interpreted from the fraction of channel fill deposit which is 6-8 m (Morris et al., 2000; Hansen et al., 2019). Bank angle is calculated from the schematic cross-section of the channel system made by Hodgson et al. (2001). The grain size distribution data is derived from the analysis of the SK-3d sample (**Figure 26**). This sample is chosen as a simulation input because of its most proximal position. The slope is assumed to be less than 2^0 (Hansen et al., 2019). However, other parameters required for modelling, such

as initial concentration and flow duration is poorly defined. In this model, we applied a range of values according to Eggenhuisen et al. (2019a). The current frequency is set for 1 and 5 turbidity events to show the application of this module in modelling bed and lobe element geometry.

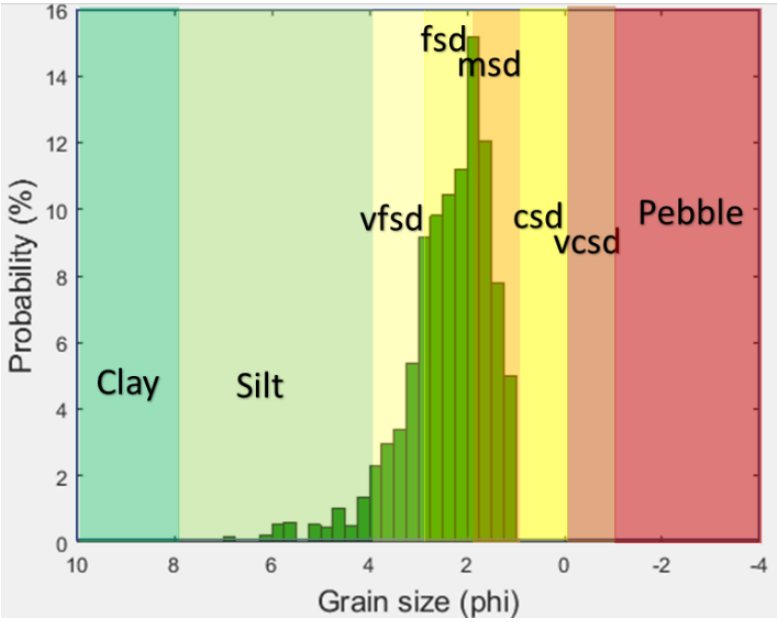

Figure 26. The grain size distribution of sample SK 3d as input data for Lobe 5 modeling. Sample position mark as a star in **Figure 24b**.

The SBE-Lobe produces the same sediment transport distance for two different current frequency conditions, 1 event and 5 events, but with a different lobe thickness (**Figure 29** and **Figure 30)**. The fine sand class is deposited up to 1.2 km, the very fine sand class is transported up to 4 km, and the silt particle is spread out to 53 km. It implies that the model predicting the lobe length within the amplitude of actual lobe length but it spatially sorts particles based on their size (**Table 8**). If we only consider the geometry the sand-rich deposits, 4 km x 2 km, the model give the predicted lobe geometry within the amplitude of the Fan-3 lobe element dimension (Prélat et al., 2009, **Figure 27**). This supports the argument that the simplified model can be applied in lobe element modeling.

Table 8. Comparison of sediment transport distance of different particles size between model and experiment

Grain Size Class	Transport Distance (km)	
	Field data	Model
Silt	2.5*	53
v.f. sand		3.9
f. sand		1.2
m. sand	-	0.5

* Minimum sediment transport distance from the field observation

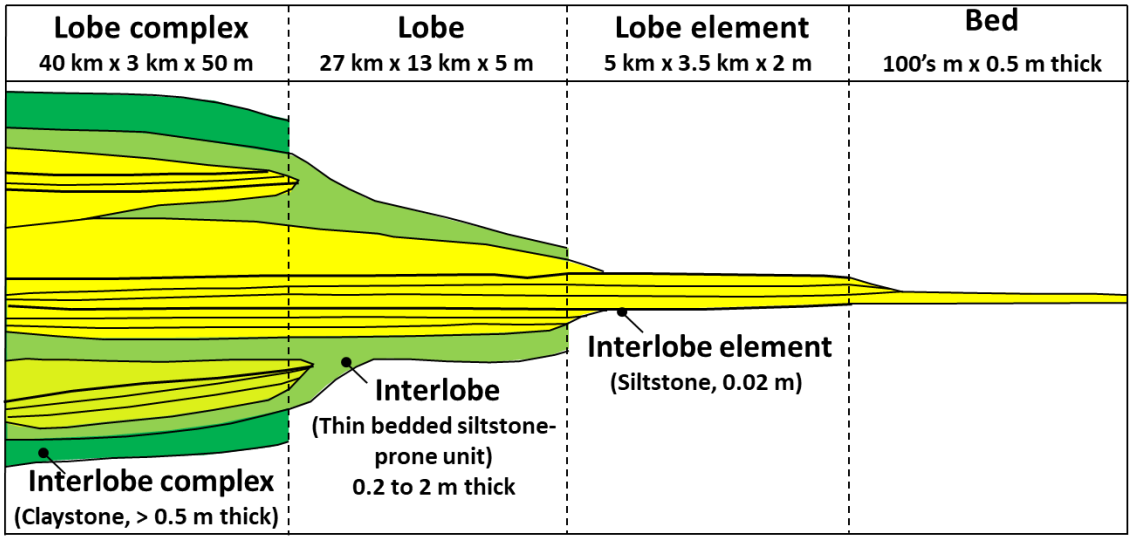

Figure 27. The schematic hierarchical unit developed from the Fan 3 lobe complex (modified from Prélat et al., 2009).

Using the P50 sediment budget estimation, the average thickness of the middle lobe from 1 and 5 turbidity events is 4 cm 20 cm respectively (**Table 9**). If we used the P90 sediment budget estimation, the predicted lobe thickness increase by 5 folds to 21 cm for 1 turbidity event and 100 cm for 5 turbidity events. The sediment budget estimation for this system is shown in **Figure 28**.

In comparison to the field data, the model predict the bed thickness within the amplitude of field data, but with 5 turbidity currents, it produces significant thinner lobe element (**Table 9**). The main uncertainty in modeling the lobe element thickness is determining how many turbidity current events that constructed the sequences observed in the field. Based on this result, it suggest that the lobe element of Lobe-5 is constructed by more than 5 turbidite events.

This result demonstrates the potential of the SBE-Lobe to be used to estimate how many of your turbidity current deposits are needed to deposit the full thickness observed in the field.

Table 9. Comparison of Lobe-5 thickness from field observation and the model using the P50 sediment budget estimation

Distance from reference point Log SK 1	Lobe thickness [m]	Lobe element thickness range [m]	Bed thickness range [m]	1 turbidity current		5 turbidity current	
				Model [m]	Ratio to lobe thickness	Model [m]	Ratio to lobe thickness
0	5.1	0.2 - 2.6	0.01 - 0.25	0.488	9.6%	2.431	47.7%
210	6.7			0.101	1.5%	0.502	7.5%
860	5.2			0.052	1.0%	0.259	5.0%
1160	6.6			0.040	0.6%	0.200	3.0%
1280	3.7			0.036	1.0%	0.178	4.8%
1400	6.5			0.033	0.5%	0.166	2.5%
1490	4.8			0.032	0.7%	0.157	3.3%
1720	1.9			0.024	1.3%	0.121	6.4%
2000	2.3			0.019	0.8%	0.096	4.2%
2240	0.9			0.013	1.5%	0.066	7.3%
2350	1.4			0.013	0.9%	0.063	4.5%
2560	0.9			0.012	1.3%	0.058	6.4%

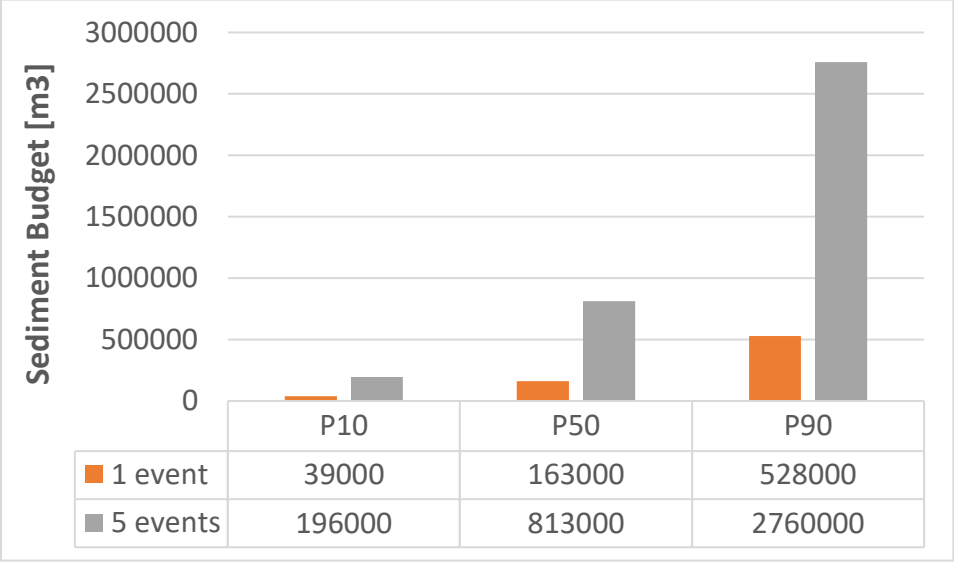

Figure 28. Sediment budget estimation of Lobe 5, Fan 3 of Skoorsteenberg Formation

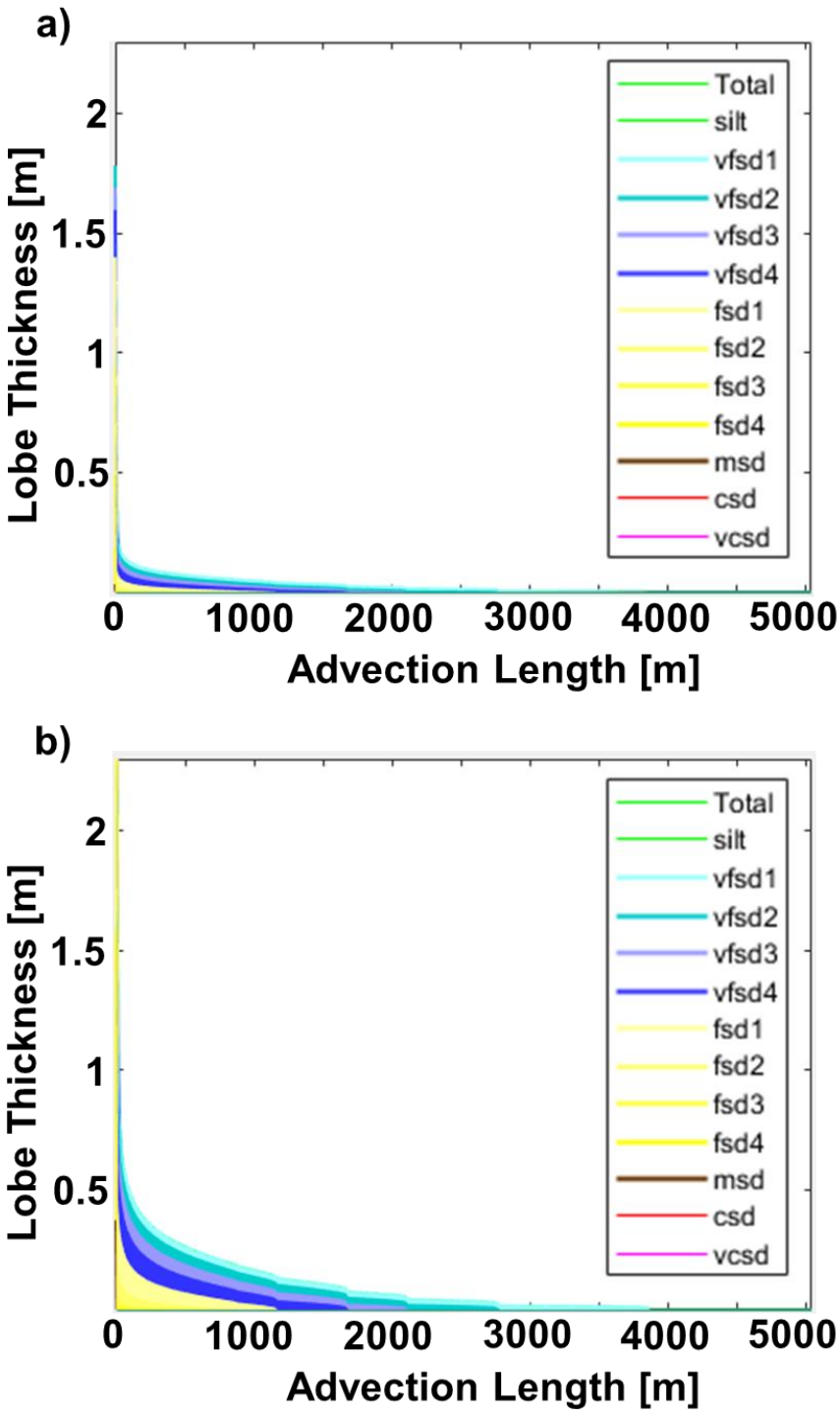

Figure 29. The predicted fan lobe geometry Lobe 5, Fan 3, Skoorsteenberg Formation that formed from 1 turbidity event, a) Using P10 sediment budget estimation, b) Using P90 sediment budget estimation

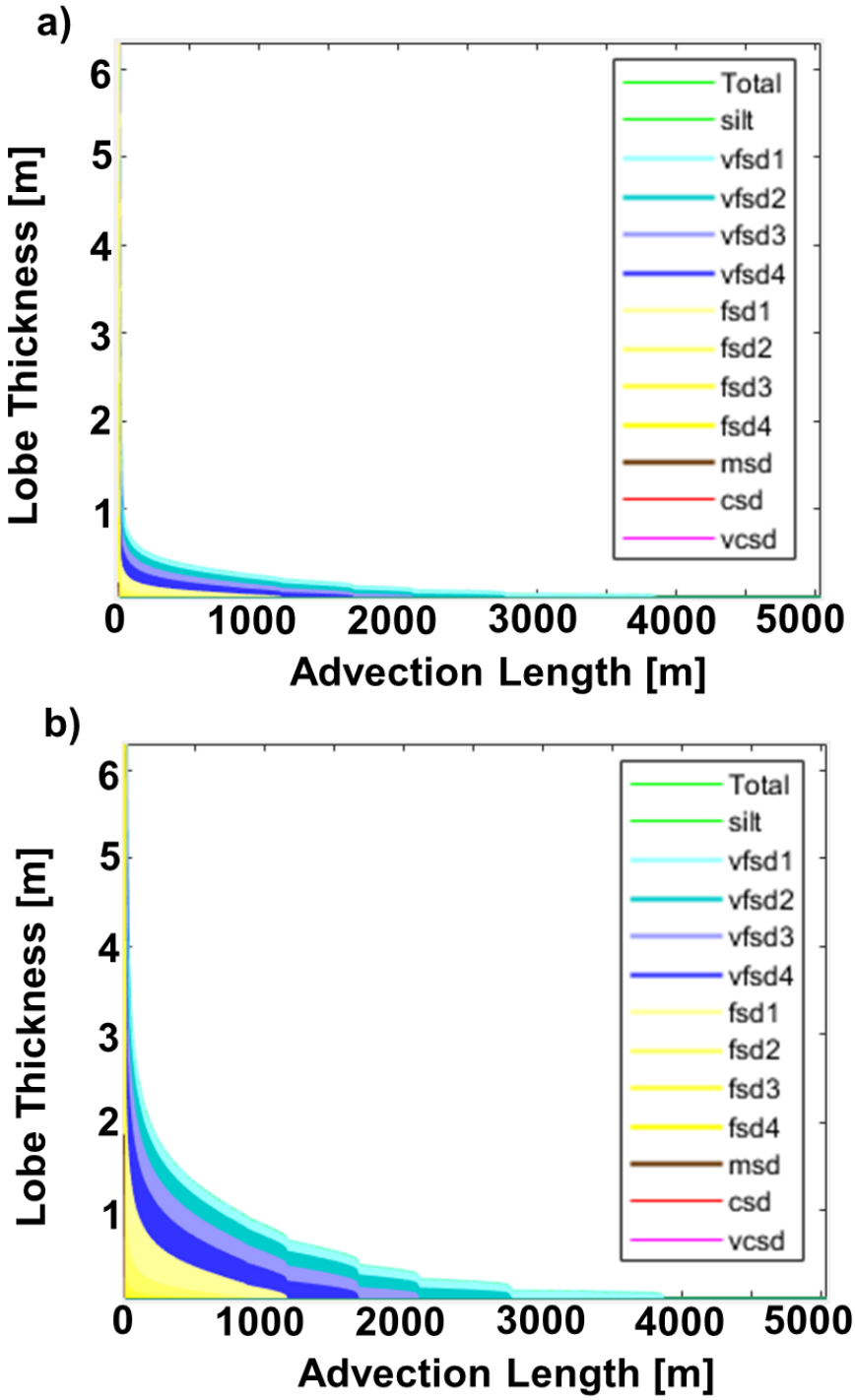

Figure 30. The predicted fan lobe geometry Lobe 5, Fan 3, Skoorsteenberg Formation that formed from 5 turbidity events, a) Using P10 sediment budget estimation, b) Using P90 sediment budget estimation

4.3. Discussion about the SBE-Lobe Application to Ancient Turbidite Deposits

The application of the SBE-Lobe to the ancient turbidite deposit has shown its consistency in predicting the sediment budget and the ability to predict the submarine lobe geometry and the average grain-size distribution based on the channel system within the amplitude of field data. From the modeling result, the fine sediment relatively has a uniform thickness and widely spread out to the distal area. This type of uniform layer is commonly found in the outcrop of turbidite system. An explanation for this observation may be due to the different settling rates of the turbidity clouds. This mechanism mentioned by Hansen et al., (2019) that fine grain material is being deposited as a result of a dilute current. While the coarse material (fine sand and larger grain particle) is thicker in the proximal area and thinning or pinch-out toward the basin. The pinch-out of the sand layer also generally found in the natural system, such as in Lobe 4, Fan 3 of Skootersberg Formation, Karoo Basin (Hansen et al., 2019).

One limitation of studying the submarine lobe through field observation is the lobe systems are commonly larger than ancient outcrops. Consequently, local 1D sections are typically used to construct their 3D geometry (Prélat et al., 2010). Here, the SBE-Lobe can be applied to predict the lobe geometry, provide a perspective of the flow structure on turbidity currents responsible for respective lobe deposits. In addition to that, this tool can be used to estimate how many turbidity current deposits that make up the lobe element.

The SBE-Lobe also has the potential to be applied in the subsurface evaluation, in particular when the existing subsurface datasets have limitations in defining the lobe geometry. Such as lack of spatial distribution of well data and poor seismic image. The SBE-Lobe can be used as the first order estimation for the gross reservoir volume, localize the potential area, and defining the reservoir boundary.

The geological parameters required for the simulation are feeder channel geometry including its slope gradient, the grain size distribution data of channel deposit, and turbidity recurrence time. The channel geometry and slope gradient can be obtained from the seismic while the turbidity recurrence time can be based on the user's understanding of the particular system (Eggenhuisen et al., 2019a). For the grain size distribution, it can be derived from core data, sidewall core (SWC), or cuttings. Taking the grain size distribution data from an analog model

(E.g outcrops data) also can be an alternative source of grain size data if the well data are not available.

However, data integration is still required to deliver accurate reservoir quality distribution of lobe systems. Pilot testing of the SBE-Lobe into the real subsurface data is also needed to further assess its accuracy and limitation before it fully applied in the subsurface evaluation.

5. Conclusions

Integration of the Rouse Equation for all grain size classes is enabling us to develop the new version of SBE-Channel to generate the sediment concentration profile that considering the way different grain sizes distribute vertically on the suspended sediment transport. Despite its limitation in calculating the fine particle size sediment budget of turbidity current deposit, the application of this equation allows us to further develop the SBE-Lobe Module. In terms of the level of the hierarchy, the model generated by the new module can be compared against the bed and lobe element geometries that comprise of weakly compensational beds.

Model validation against laboratory experiments has revealed that this tool can be used as the first-order prediction of lobe geometry. It gives a relatively good estimation of lobe thickness in the middle and the distal area. Furthermore, it also can locate the area where the fine sand grain size class, which is promising for reservoir candidate, is mainly deposited. A better understanding of the geological condition will lead to better modeling accuracy. We also show that lobe length is proportional to the slope of the channel system, the flow thickness, and a fraction of grain particles, but not to the sediment volume.

The application of the SBE-Lobe to the ancient turbidite deposit has shown its consistency in predicting the sediment budget and its ability to predict the submarine lobe geometry and the average grain-size distribution based on the channel system within the amplitude of field data. The SBE-Lobe also has the potential to be applied to model and predict lobe characteristics in subsurface settings, especially where these are often poorly constrained by seismic and well data. The SBE-Lobe can be used as the first order estimation for the gross reservoir volume, localize the potential area, and defining the reservoir boundary.

However, this version of SBE still has limitation especially in predicting the apex lobe geometry. The model tends to overpredict the lobe thickness in the proximal area and underpredict the sediment transport distance of the coarser particle. Therefore, future research should aim to improve the tool by integrating the dynamic process that occurs in the CLTZ into the model and coupling the effect of the temporal and spatial evolution of the flow velocity. Pilot testing of the SBE-Lobe into the real subsurface data is also needed to further assess its accuracy and limitation before it fully applied in the subsurface evaluation.

References

Altinakar, M. S., Graf, W. H., and **Hopfinger, E. J.** (1996). Flow structure in turbidity currents. *Journal of Hydraulic Research, 34*(5), 713-718.

Berends, S. H. (2018). *Grain size analysis by thin section images of Permian deep-marine sediments from the Fort Brown Formation, Karoo Basin, South Africa* (Master's thesis). Universiteit Utrecht, Utrecht, The Netherlands

Boggs Jr, S., and **Boggs, S**. (2009). Petrology of sedimentary rocks. Cambridge University Press.

Eggenhuisen, J. (unpublished). The EuroSEDS Sediment Budget Estimator (SBE); integrating a turbidity current process model in Source-to-Sink sediment budget estimates.

Bolla Pittaluga, M. and **Imran, J.** (2014) A simple model for vertical profiles of velocity and suspended sediment concentration in straight and curved submarine channels. *Journal of Geophysical Research: Earth Surface*, 119, 483–503. https ://doi.org/10.1002/2013J F0028 12.

Bouma, A.H. (2000). Fine-grained, mud-rich turbidite systems: Model and comparison with coarse-grained, sand-rich systems. In: *Fine-grained Turbidite Systems* (Eds. A.H. Bouma and C.G. Stone) *AAPG Memoir 72/SEPM Spec. Publ.*, 68, 9-19.

de Leeuw, J., Eggenhuisen, J.T., Spychala., Y.T., Heijnen, M.S., Pohl, F. and **Cartigny, M.J.B**. (2018). Sediment Volume and Grain-Size Partitioning between Submarine Channel-Levee Systems and Lobes: An Experimental Study. *J. Sed. Res*., **88**, 1-18

Deptuck, M.E., Piper, D.J.W., Savoye, B. and **Gervais, A.** (2008). Dimensions and architecture of late Pleistocene submarine lobes off the northern margin of East Corsica. *Sedimentology*, **55**, 869-898.

Deptuck, M. E., and **Sylvester, Z**. (2018). Submarine Fans and Their Channels, Levees, and Lobes. Submarine Geomorphology Springer Geology, 273–299. doi: 10.1007/978-3-319-57852-1_15

Eggenhuisen, J. T., Cartigny, M. J. B., and de Leeuw, J. (2017). Physical theory for near-bed turbulent particle suspension capacity, Earth Surf. Dynam., 5, 269–281, https://doi.org/10.5194/esurf-5-269-2017

Eggenhuisen, J.T., de Leeuw, J., Pohl, F., Spychala, Y., Tilston, M.C., Heijnen, M., Wróblewska, S., Berends, N. and M.J.B. Cartigny (2019a). Final report of the Eurotank Studies of Experimental Deepwater Sedimentology (EuroSEDS), Department of Earth Sciences, Utrecht University, the Netherlands, 430pp.

Eggenhuisen, J. T., Tilston, M. C., de Leeuw, J., Pohl, F., and **Cartigny, M. J. B.** (2019b). Turbulent diffusion modelling of sediment in turbidity currents; an experimental validation of the Rouse approach. *The Depositional Record*

Ferguson, R.I., and **Church, M.,** (2004). A simple universal equation for grain settling velocity. *Journal of Sedimentary Research*, 74, 933–937. doi:10.1306/051204740933

Fildani, A., Normark, W.R. (2004). Late Quaternary evolution of channel and lobe complexes of Monterey Fan. Marine Geology 206, 199–223.

Ganti, V., Lamb, M.P. and **McElroy, B.** (2014). Quantitative bounds on morphodynamics and implications for reading the sedimentary record. *Nature Comm.*, **5**, Article number: 3298

Garcia, M. (2008). Sedimentation engineering: processes, measurements, modeling, and practice. *ASCE*.

Grundvåg, S.A., Johannessen, E.P., Helland-Hansen, W. and **Plink-Björklund, P.** (2014). Depositional architecture and evolution of progradationally stacked lobe complexes in the Eocene Central Basin of Spitsbergen. *Sedimentology*, **61**, 535-569.

Hansen, L. A.S., Hodgson, D.M., Pontén, A., Bell, D. and **Flint, S.** (2019). Quantification of Basin-Floor Fan Pinchouts: Examples from the Karoo Basin, South Africa. *Front. Earth Sci*. 7:12. doi: 10.3389/feart.2019.00012

Hamilton, P., Gaillot, G., Strom, K., Fedele, J. and **Hoyal., D.** (2017). Linking hydraulic properties in supercritical submarine distributary channels to depositional-lobe geometry. *J. Sed. Res*., **87**, 935-950.

Hiscott, R.N., Hall, F.R. and **Pirmez, C.** (1997) Turbidity-current overspill from the Amazon Channel: texture of the silt/sand load, paleoflow from anisotropy of magnetic susceptibility and implications for flow processes. *Proceedings of the Ocean Drilling Porgram, Scientific Results*, 155, 53–78. https://doi.org/10.2973/odp.proc.sr.155.202.1997

Jobe, Z. R., Howes, N., Romans, B. W., and **Covault, J. A**. (2018). Volume and recurrence of submarine-fan-building turbidity currents. *The Depositional Record.*

Kane, I.A., Pontén, A.S.M., Vangdal, B., Eggenhuisen, J.T., Hodgson, D.M. and **Spychala, Y.T.** (2017). The stratigraphic record and processes of turbidity current transformation across deep-marine lobes. *Sedimentology*, **64**, 1236–1273

King, R.C., Hodgson, D.M., Flint, S.S., Potts, G.J. and Van Lente, B. (2009) Development of subaqueous fold belt as a control on the timing and distribution of deep water sedimentation: an example from the Southwest Karoo Basin, South Africa. In: External Controls on Deep- Water Depositional Systems (Eds B. Kneller, O.J. Martinsen and B. McCaffrey), *SEPM Special Publication*, 92, 261–278.

Komar, P. (1971). Hydraulic jumps in turbidity currents. *Geol. Soc. Am*. Bull. 82, 1477–1488. doi: 10.1130/0016-7606197182.

Macauley, R. V., & Hubbard, S. M. (2013). Slope channel sedimentary processes and stratigraphic stacking, Cretaceous Tres Pasos Formation slope system, Chilean Patagonia. *Marine and Petroleum Geology*, 41(1), 146–162. https://doi.org/10.1016/j.marpetgeo.2012.02.004.

Mohrig, D., and **Buttles, J**. (2007). Deep turbidity currents in shallow channels. *Geology*, *35*(2), 155-158.

Mulder, T. and **Alexander, J.** (2001). Abrupt change in slope causes variation in the deposit thickness of concentrated particle-driven density currents. *Mar. Geol*., **175**, 221-235.

Mutti, E. (1977). Distinctive thin-bedded turbidite facies and related depositional environments in the Eocene Hecho Group (South-central Pyrenees, Spain). *Sedimentology*, **24**, 107-131.

Mutti, E. and **Normark, W.R.** (1987). Comparing examples of modern and ancient turbidite systems: Problems and concepts. *In: Marine Clastic Sedimentology: Concepts and Case Studies* (Eds. J.K. Leggett and C.G. Zuffa) Graham & Trotman, London, 1-38.

Novianti, W. (2019). *An Analytical Model to Predict the Sediment Flux of Each Grain-Size Class in Turbidity Current Flow; Application to Gold Channel, Tres Pasos Formation, Chile* (Master's thesis). Universiteit Utrecht, Utrecht, The Netherlands

Pettinga, L., Jobe, Z., Shumaker, L., and **Howes, N.** (2018). Morphometric scaling relationships in submarine channel–lobe systems. *Geology* ; 46 (9): 819–822. doi: https://doi.org/10.1130/G45142.1

Pohl, F. (2019). *Turbidity currents and their deposits in abrupt morphological transition zones* (Doctoral dissertation, UU Dept. of Earth Sciences).

Pohl, F., Eggenhuisen, J., Tilston, M., & **Cartigny, M.** (2019). New flow relaxation mechanism explains scour fields at the end of submarine channels. *Nature Comm*., doi: 10.31223/osf.io/buknq

Porten, K.W., Kane, I.A., Warchoł, M.J. and **Southern, S.J.** (2017). A sedimentological process-based approach to depositional reservoir quality of deep-marine sandstones: an example from the Springar Formation, north-western Vøring Basin, Norwegian Sea. *J. Sed. Res*., **86**, 1269-1286.

Prélat, A., Hodgson, D.M. and **Flint, S.S.** (2009). Evolution, architecture and hierarchy of distributary deep-water deposits: a high-resolution outcrop investigation from the Permian Karoo Basin, South Africa. *Sedimentology*, **56**, 2132-2154.

Prélat, A., Covault, J.A., Hodgson, D.M., Fildani, A. and **Flint, S. S.** (2010). Intrinsic controls on the range of volumes, morphologies, and dimensions of submarine lobes. *Sed. Geol*., **232**, 66-76.

Prélat, A. and **Hodgson, D.M.** (2013). The full range of turbidite bed thickness patterns in submarine lobes: controls and implications. *J. Geol. Soc. London*, **170**, 1-6.

Reading, H. G. and **Richards, M. (1994).** Turbidite Systems in Deep-Water Basin Margins Classified by Grain Size and Feeder System. *AAPG Bulletin*; 78 (5): 792–822. doi: https://doi.org/10.1306/A25FE3BF-171B-11D7-8645000102C1865D

Rouse, H., 1937. Modern Conceptions of the Mechanics of Fluid Turbulence. Transactions of the American Society of Civil Engineers, 102, 463–505

Smith, R.H.M. (1990). A review of stratigraphy and sedimentary environments of the Karoo basin of South Africa. J. Afr. *Earth Sc.*, 10, 117–137.

Spychala, Y., Eggenhuisen, J., Tilston, M., and **Pohl, F.** (2019). The influence of basin settings and flow properties on the dimensions of submarine lobe elements. *Sedimentology*. doi: 10.31223/osf.io/sk8v3

Spychala, Y.T., Hodgson, D.M., Prélat, A., Kane, I.A., Flint, S.S. and **Mountney, N.P.** (2017a). Frontal and Lateral Submarine Lobe Fringes: Comparing Sedimentary Facies, Architecture and Flow Processes. *J. Sed. Res.*, **87**, 75-96.

Straub, K. M. and **Mohrig, D.** (2008). Quantifying the morphology and growth of levees in aggrading submarine channels. *Journal of Geophysical Research: Earth Surface*, *113*, 1–20. https ://doi.org/10.1029/2007J F000896.

Straub, K. M. and **Pyles D. R.** (2012). Quantifying the hierarchical organization of compensation in submarine fans using statistics. *J. Sed. Res* v. 82, 889–898.

Sylvester, Z., and **Lowe, D. R**. (2004). Textural trends in turbidites and slurry beds from the Oligocene flysch of the East Carpathians, Romania. *Sedimentology*, 51(5), 945-972.

van Rijn (1993). Principles of sediment transport in rivers, estuaries and coastal seas. *Aqua Publications*, Amsterdam, the Netherlands, pp.715

Wynn, R. B., Weaver, P.P.E, Masson, D. G., and **Stow, D. A. V.** (2012). Turbidite depositional architecture across three interconnected deep-water basins on the north-west African margin. *Sedimentology*, 49, 669–695

Appendixes

Appendix 1. Simulation Parameter for Model Development

Parameter	Value	Remarks
The density of water (ρ_w)	1000	kg/m^3
The density of quartz (ρ_s)	2650	kg/m^3
Dynamic viscosity of water (μ)	$1.3x10^{-3}$	Kg/ms, At $T=10^0C$
Kinematic viscosity of water (v)	$1.3\ x10^{-6}$	m^2/s; at $T=20^0C$; $v = \mu / v$
Gravity Acceleration (g)	9.81	m/s^2
Von Karman's constant (K)	0.4	[-]
Proportional coefficient between turbulent and sediment diffusivity (ß)	1	[-]
Constant in Stokes' equation for laminar settling (C1)	18	[-]
Constant drag coefficient (C2)	1	[-]

Appendix 2. Variables used in the sensitivity analysis in the section 2.2.3

	Base Condition						
Parameters	**Min**	**Max**	**Max-min**	**Increased by 20%**	**P90-P10**	**Decreased by 20%**	**P90-P10**
Channel width [m]	300	600	300	660	4,621,084	540	3,705,923
Channel Height [m]	10	20	10	22	4,561,640	18	3,522,710
Slope [%]	1.5	3	1.5	3.3	4,281,582	2.7	4,025,423
Current Duration [hrs.]	3	6	3	6.6	4,441,076	5.4	3,833,115
Initial Concentration [%]	0.3	0.6	0.3	0.66	4,564,668	0.54	3,757,242

Appendix 3. Grain-size distribution and sediment concentration profile of sample AX-180 and AX-30

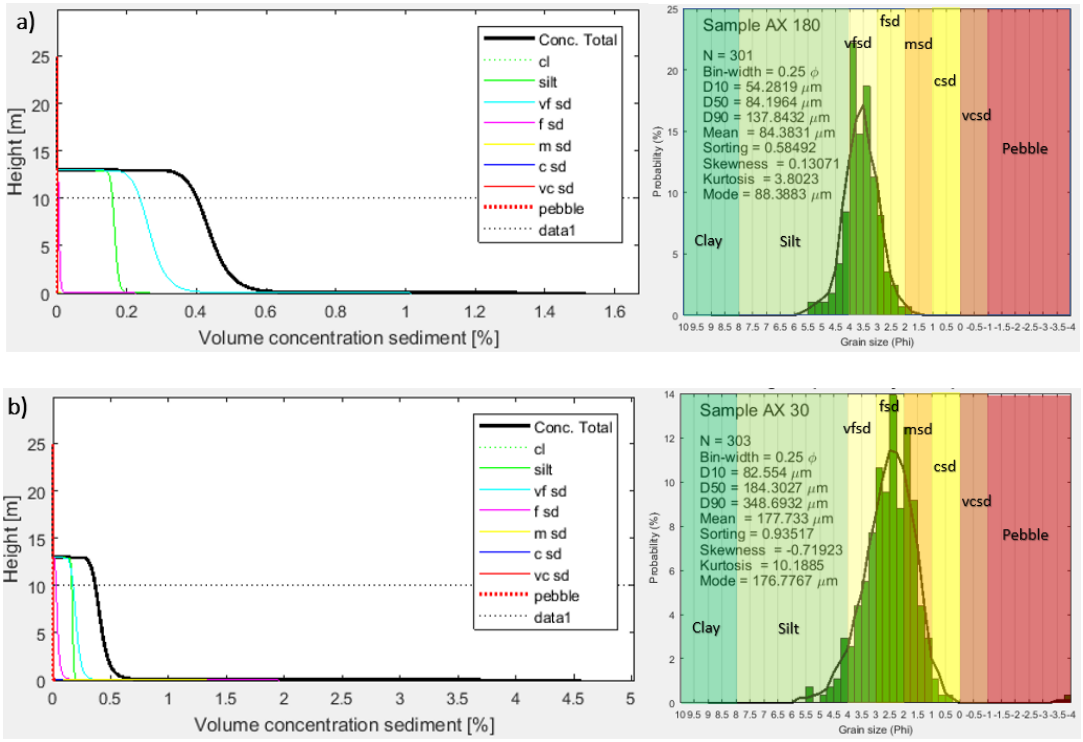

Appendix 4. Grain-size distribution of axis channel deposits, Gold Channel